GAVIN PUBLISHERS

Archives of Natural and Medicinal Chemistry

Zamakshshari NH, et al. Arch Nat Med Chem 2017: ANMC-110.

Research Article

DOI: 10.29011/ANMC-110.000010

Cytotoxic Activities of Anthraquinones from *Morinda citrifolia* towards SNU-1 and LS-174T and K562 Cell Lines

Nor Hisam Zamakshshari[1], Gwendoline Cheng Lian Ee[1*], Siau Hui Mah[2], Zalikha Ibrahim[3], Soek Sin Teh[4] , Shaari Daud[1]

[*1]Department of Chemistry, University Putra Malaysia, Malaysia

[2]School of Biosciences, Taylor's University, Malaysia

[3]Department of Pharmaceutical Chemistry, International Islamic University, Malaysia

[4]Energy and Environment, Malaysia Palm Oil Board, Malaysia

[*]**Corresponding author:** Gwendoline Cheng Lian Ee, Department of Chemistry, University Putra Malaysia, Malaysia. Tel: +60389466785; Email: gwen@upm.edu.my

Citation: Zamakshshari NH, Lian Ee GC, Mah SH, Ibrahim Z, Teh SS, et al. (2017) Cytotoxic Activities of Anthraquinones from *Morinda citrifolia* towards SNU-1 and LS-174T and K562 Cell Lines. Arch Nat Med Chem 2017: ANMC-110. DOI: 10.29011/ANMC-110.000010

Received Date: 28 November, 2017; **Accepted Date:** 9 December, 2017; **Published Date:** 28 December, 2017.

Abstract

Background: Plants have been used in medicine for a long time by human civilization to cure diseases. Most of the drugs in clinical use are from natural products including chemotherapeutic drugs.

Method: Twelve anthraquinone derivatives were successfully isolated from *Morinda citrifolia* and tested for their cytotoxic activities against stomach cancer cell line, SNU-1, colon cancer cell line, LS-174T and leukaemia cell line, K562. A molecular docking study was performed on three potential protein receptors, HER-2 (PDB ID: 3PP0), β-catenin (PDB ID: 1JDH) and Src protein kinase (PDB ID: 2SRC), in order to model the probable binding interaction between isolated compounds towards the respective protein receptors.

Result: Morindone (**4**) showed the highest cytotoxic activities against SNU-1 and LS-174T cell lines with IC_{50} values of 2.72 µg/ml and 2.93 µg/ml, respectively. Meanwhile, nordamnacanthal **(1)** showed the highest cytotoxic activity against K562 with IC_{50} value of 5.99µg/ml. The structure-activity relationship studies showed that the presence and arrangements of formyl, hydroxyl and methoxyl substituents in the anthraquinone skeleton are important towards the cytotoxic activities. Molecular docking studies showed all the active compounds could bind well with the responsible protein.

Conclusion: Some anthraquinone compounds isolated from *Morinda citrifolia* were determined and could act as anti-cancer inhibitors for SNU-1, LS-174T and K562.

Keywords: Anthraquinone; K562; LS-174T; *Morinda citrifolia*; Molecular Docking; SNU-1, Structure Relationship Activity

Introduction

The genus *Morinda* belongs to the Rubiaceae family. This genus consists of about 80 species, mostly of old World origin [1]. In Malaysia, *Morinda* comprises nine species which include three species of trees and six species of climber [2]. *Morinda* is known to be used in traditional folk medicine for treatment of many diseases such as diabetes, hypertension, and cancer [3]. The species of *Morinda morindoides* is important in Liberian traditional medicine for treating malaria, fever and worm infestations [4]. A research that was performed on *Morinda lucida* reported positive results towards lowering glucose level on streptozotocin-treated rats [5]. Most *Morinda* species are enriched with active phenolic compounds including anthraquinones which explains its biological activities [6] such as anti-inflammation, antioxidant, lipoxygenase inhibition, inhibition of cell transformation and quinone reductase-inducing activity [7].

Cancer is a major cause of death worldwide. According to a World Health Organization survey in 2015, about 8.8 million cases of deaths have been reported due to cancer [8]. Colon and stomach cancer are listed as the most common cause of cancer-related death with 774,000 and 754,000 deaths, respectively [8]. These cancers are the most common type of cancer diseases in both genders

[9]. Researches regarding to these types of cancer are less when compared to breast and cervical cancer [10]. Colon and stomach cancer differ in terms of their involvement in signaling pathway. In stomach cancer, amplification or overexpression of HER2 in HER/EGFR of approximately 10-30% was reported. This significant amplication of HER2 has served as a prognostic and predictive biomarker for stomach cancer [11]. Meanwhile, colon cancer was reported to have a connection with the increase of β-catenin level in Wnt/β-catenin/Tcf signalling pathway, which has led to high proliferation and growth of cell cancer [12].

Meanwhile, leukemia had listed as common types of human cancer occur nowadays with 8% cases from overall cancer cases reported [13]. Leukemia is a type of cancer that defined by an abnormal and uncontrolled proliferation of one or more types of hematopoietic cell [14]. Leukemia may arise from various factor such as overexpression or inhibition of various genes, the accumulation of inhibitory mutation in proliferation-related genes and chromosomal translocation [15]. The different types of leukemia might arise from different factors. K562 cell is known as chronic myeloid leukemia that frequently occur in adults at the age of 40-50 years old and the cause of these types of cancer is still remaining [16]. Chemotherapy is one of the optional treatments used to treat leukemia by using a targeted therapy drug. In order to determined or design this targeted therapy drug, a specific biological pathway for these types of cancer needs to be understood. The previous studies had shown an overexpress of Src kinase activity had occured in leukemia, K562 cell [17,18]. Thus, suppressing the activation of Src kinase activity by targeted therapy drug might be a key to cure this disease.

Based on the above information, *Morinda citrifolia* was selected for a detail phytochemical and pharmacological investigation. In this study, 12 anthraquinones, compounds 1-12 (Figure 1), were successfully isolated from this species. All the anthraquinone compounds were tested for their cytotoxic activities towards SNU-1, LS-174T and K562 cells. The cytotoxic activities of these compound as well as structure-activity relationship of anthraquinone derivatives are predicted. In order to elucidate the potential mechanism by which the active compounds induce the cytotoxic activity, molecular docking was performed to position the compounds into the active site of HER-2 (PDB ID: 3PP0), β-catenin (PDB ID: 1JDH) and Src protein kinase (PDB ID: 2SRC).

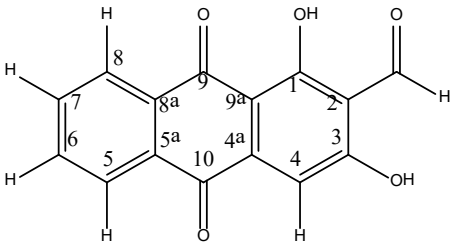

(**1**)

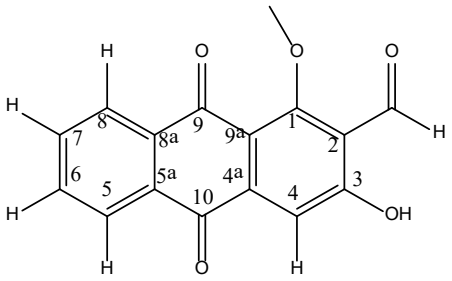

(**2**)

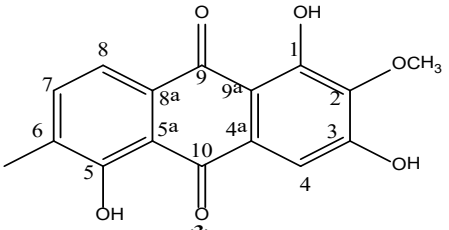

(**3**)

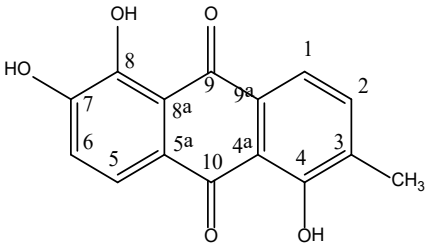

(**4**)

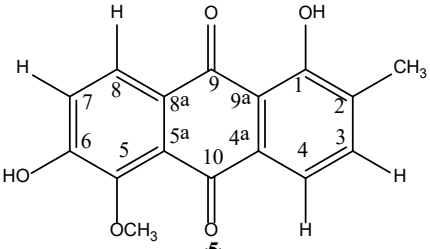

(**5**)

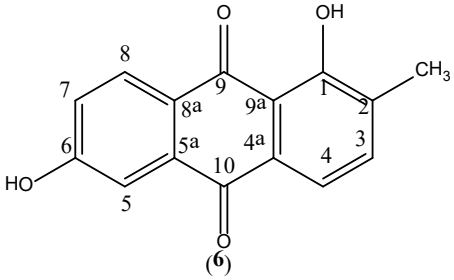

(**6**)

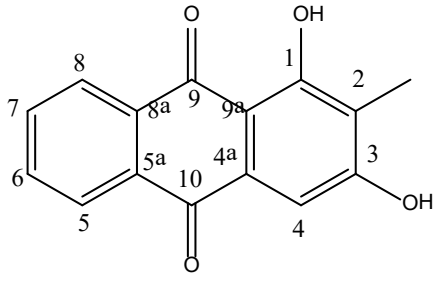

(**7**)

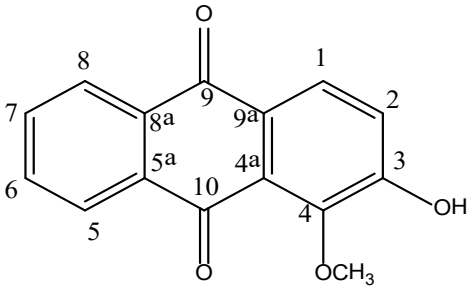

(**8**)

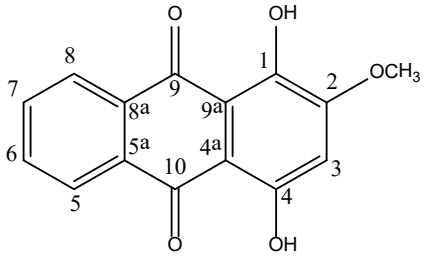

(**9**)

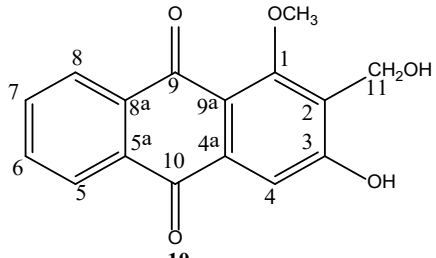

(**10**)

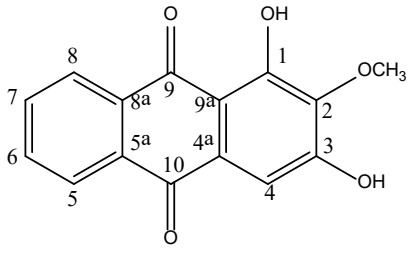

(**11**)

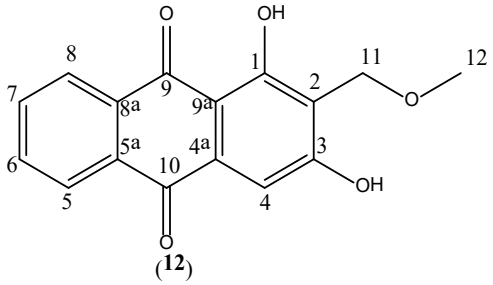

(**12**)

Figure 1: Structures of nordamnacanthal (**1**), damnacanthal (**2**), 1,3,5-trihydoxy-2-methoxy-6-methyl anthraquinone (**3**), morindone (**4**), 1,6-dihydoxy-5-methoxy anthraquinone (**5**), sorendidiol (**6**), rubiadin (**7**), alizarin (**8**), 1,4-dihydroxy-2-methoxy anthraquinone (**9**), damnacanthol (**10**), 1,3-dihydroxy-2-methoxy anthraquinone (**11**) and lucidin-ω-methylether (**12**)

Materials and Method

Chemicals

The Roswell Park Institute (RPMI 1640) and Eagle's Minimum Essential Media (MEM) used for cell culture were purchased from AMRESCO®. The Fetal Bovine Serum (FBS) and Phosphate Buffered Saline (PBS) were purchased from Thermo Scientific. All solvents and chemicals were purchased from Merck, Fisher and Sigma-Aldrich.

Plant Collection

The root bark of *Morinda citrifolia* was collected from Negeri Sembilan, Malaysia and was identified by Professor Dr. Rusea Go from the Biology Department, Faculty of Science, Universiti Putra Malaysia. A voucher specimen was deposited in the Herbarium of Biology Department, Faculty of Science, Universiti Putra Malaysia.

Plant Extraction

The collected root bark sample was dried under open air and ground into a fine powder. The powdered sample (0.9 kg) was then macerated three times in four different solvents which were hexane, dichloromethane, ethyl acetate and methanol for 72 hours each. The macerated extracts were filtered and evaporated under reduced pressure in a rotary evaporator to remove all the solvent. This resulted in solidified extracts of hexane (11g), dichloromethane (18g), ethyl acetate (19g), and methanol (35g). Two techniques were used to obtain twelve anthraquinone compounds: column chromatography (vacuum and gravity) and preparative thin layer chromatography. Five out of twelve anthraquinones were successfully isolated from the hexane crude extract. They were nordamnacanthal (**1**), damnacanthal (**2**), 1,3,5-trihydoxy-2-methoxy-6-methylanthraquinone (**3**), morindone (**4**) and 1,6-dihydoxy-5-methoxy-2-methyl anthraquinone (**5**). Meanwhile, another five anthraquinones from this species were successfully isolated from the semi polar extract (ethyl acetate

and dichloromethane). They were sorendidiol (**6**), rubiadin (**7**), alizarin (**8**), 1,4-dihydroxy-2-methoxy anthraquinone (**9**) and damnacanthol (**10**). The methanol extract furnished another two anthraquinones, 1,3-dihydroxy-2-methoxy anthraquinone (**11**) and lucidin-ω-methylether (**12**). The structures of these compounds were elucidated using spectroscopic analysis such as GCMS, IR, UV and 1D NMR.

Nordamnacanthal (1): Yellow needle crystal ($CHCl_3$); m.p. 219-222ºC (literature 218-220ºC [19]; UV (EtOH) λ max 290 and 246 nm; IR ν_{max} 2928, 1734, 1649, 1356, 1274 cm^{-1}; EIMS m/z 268 [M+], 240, 212, 184, 128, 69; ^1H and ^{13}C NMR spectra are consistent with literature [20] (Supplementary Material 1-4).

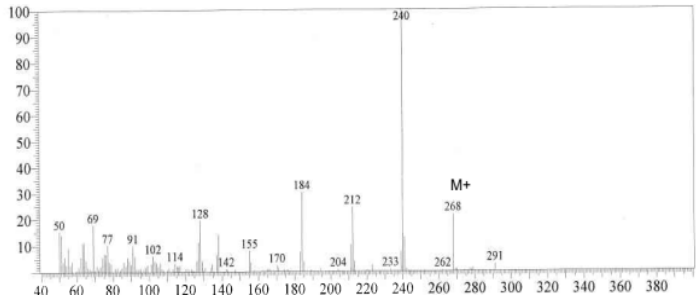

Supplementary Material 1: Eims Spectrum of Nordamnacanthal **(1).**

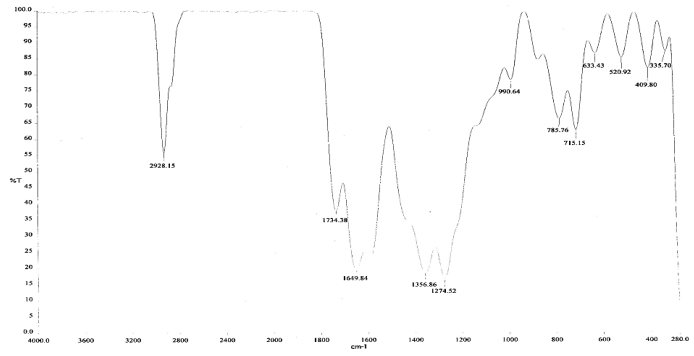

Supplementary Material 2: Ftir Spectrum of Nordamnacanthal **(1).**

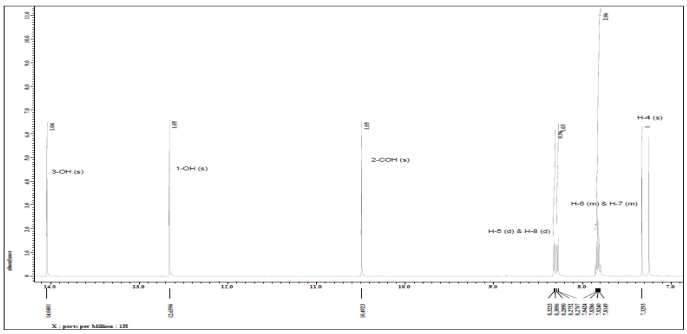

Supplementary Material 3: ^1H Nmr Spectrum of Nordamnacanthal **(1).**

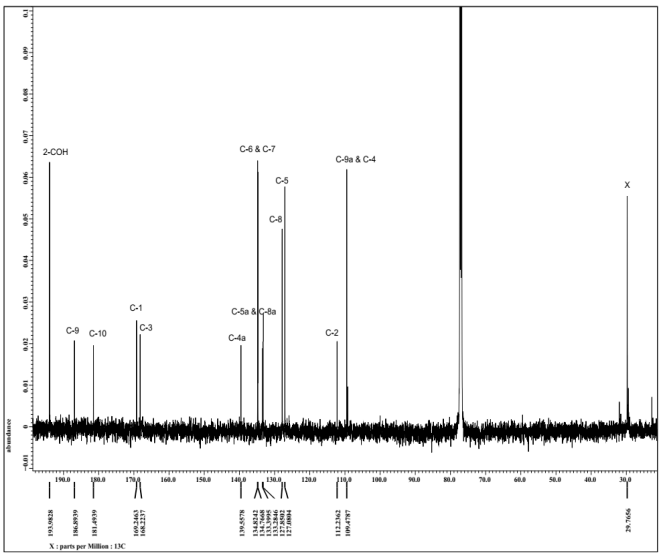

Supplementary Material 4: ^{13}C Nmr Spectrum of Nordamnacanthal **(1).**

Damnacanthal (2): Yellow needle crystal ($CHCl_3$); m.p. 208-210ºC (literature 211-212ºC, [21]); UV (EtOH) λ max 392 and 258 nm; IR ν_{max} 2927, 1664, 1441, 1282 and 1116 cm^{-1}; EIMS m/z 282 [M+], 254, 225, 208, 139, 76, 63, 50; ^1H and ^{13}C NMR spectra are consistent with literature [20] (Supplementary Material 5-8).

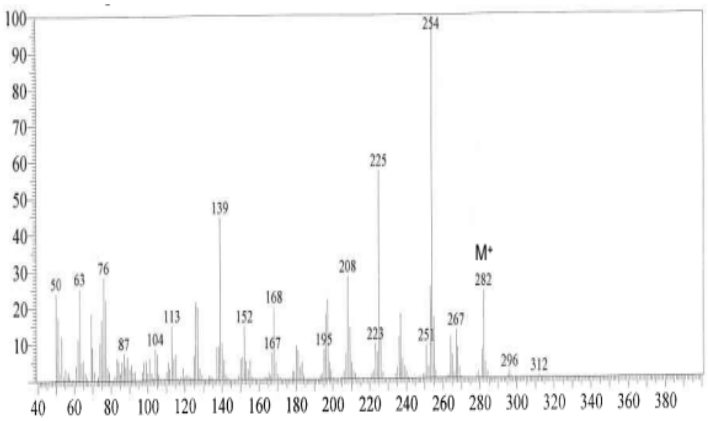

Supplementary Material 5: Eims Spectrum of Damnacanthal **(2).**

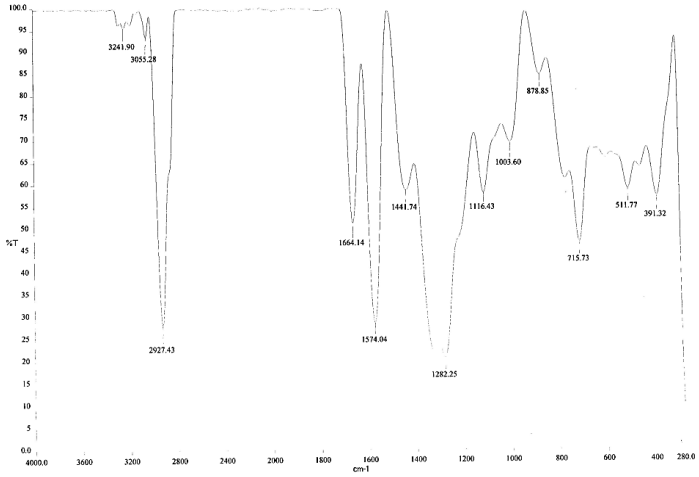

Supplementary Material 6: Ftir Spectrum of Damnacanthal **(2).**

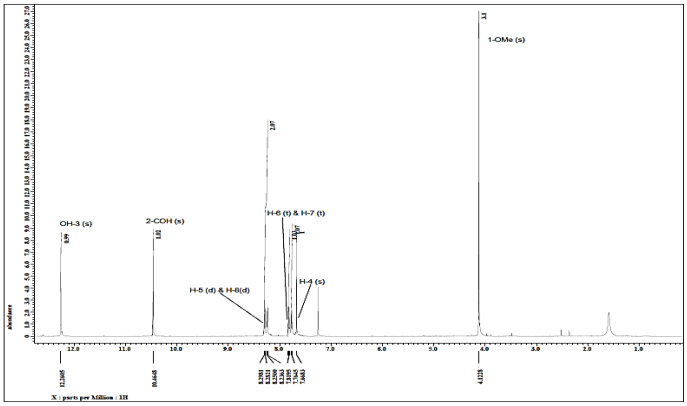

Supplementary Material 7: ^{1}H NMR Spectrum of Damnacanthal **(2).**

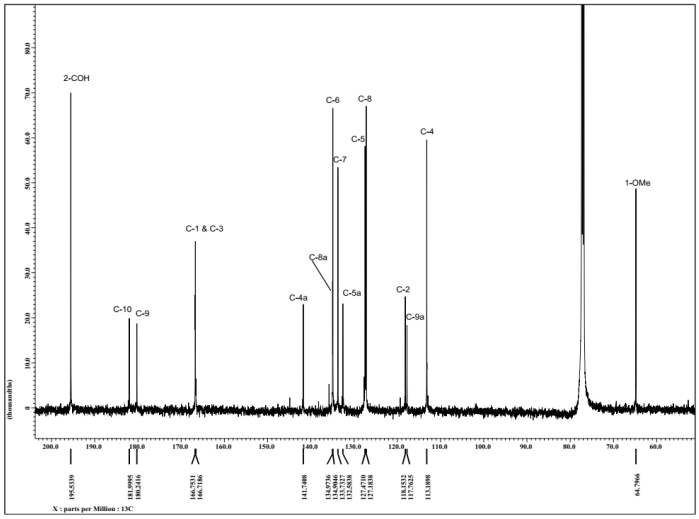

Supplementary Material 8: ^{13}C NMR Spectrum of Damnacanthal **(2)**

1,3,5-trihydoxy-2-methoxy-6-methyl anthraquinone (3): Yellow powder ($CHCl_3$); m.p. 235-239ºC (literature 241ºC [19]); UV (EtOH) λmax 412 and 302 nm; IR ν_{max} 3405, 2931, 1737, 1406, 1259 and 1161 cm^{-1}; EIMS m/z 300 [M+], 282, 257, 135, 115, 77, 63, 51; ^{1}H and ^{13}C- NMR spectra are consistent with literature [19] (Supplementary Material 9-12).

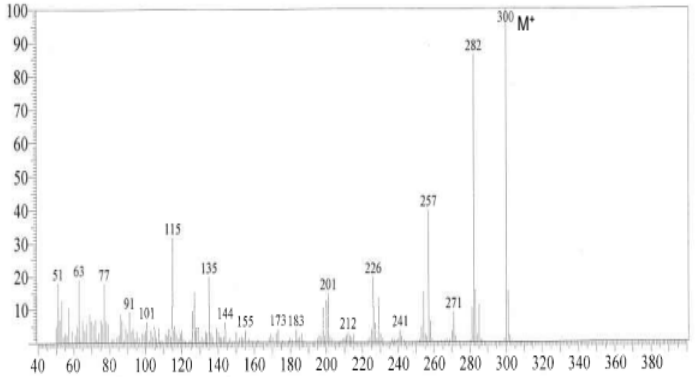

Supplementary Material 9: Eims Spectrum of 1,3,5-Trihydoxy-2-Methoxy-6-Methyl Antraquinone **(3).**

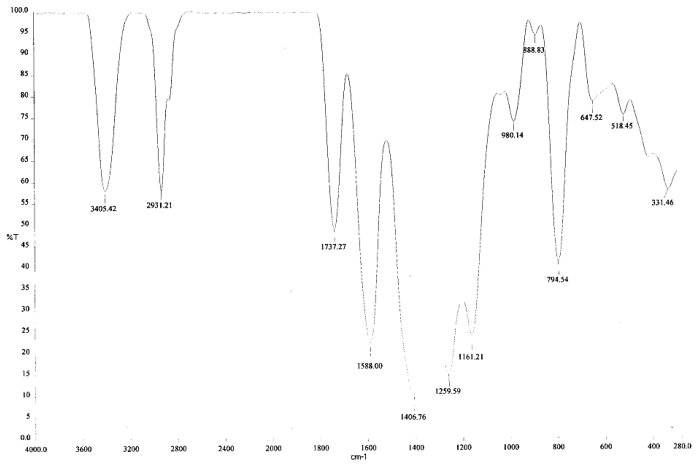

Supplementary Material 10: Ftir Spectrum of 1,3,5-Trihydoxy-2-Methoxy-6-Methyl Anthraquinone **(3).**

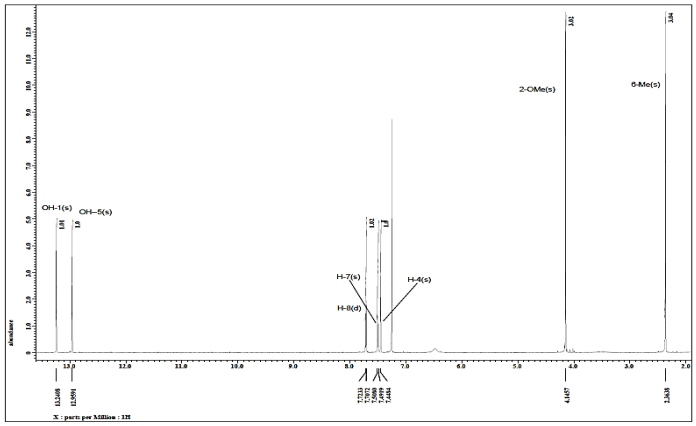

Supplementary Material 11: ^{1}H Nmr Spectrum of 1,3,5-Trihydoxy-2-Methoxy-6-Methyl Antraquinone **(3).**

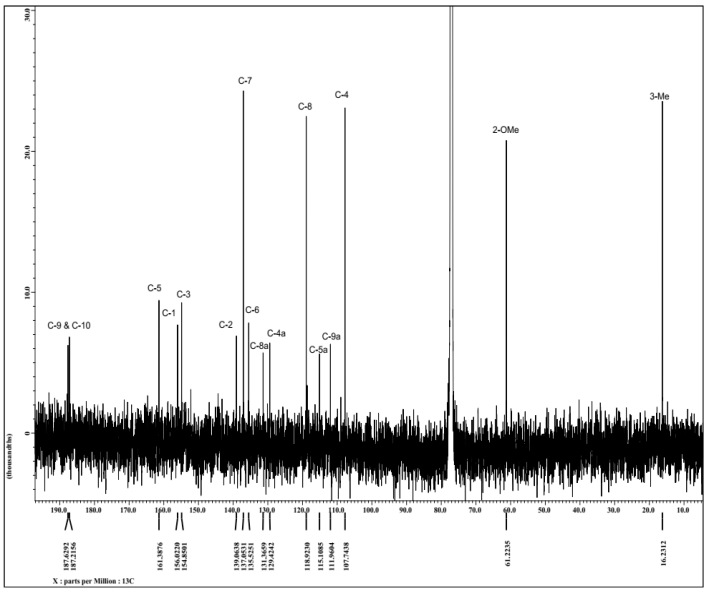

Supplementary Material 12: ^{13}C Nmr Spectrum of 1,3,5-Trihydoxy-2-Methoxy-6-Methyl Antraquinone **(3).**

Morindone (4): Orange-red needle crystal (Acetone); m.p. 248-250ºC (literature 250-251ºC, [22]; UV (EtOH) λmax 422 and 269 nm; IR ν_{max} 2919, 2854, 1597, 1273 and 1072 cm^{-1}; EIMS m/z 270 [M+], 242, 139, 77, 69, 51; ^{1}H and ^{13}C NMR spectra are consistent with literature [20] (Supplementary Material 13-16).

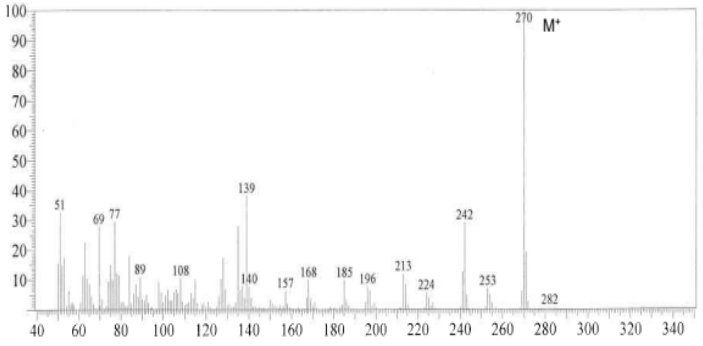

Supplementary Material 13: Eims Spectrum of Morindone **(4).**

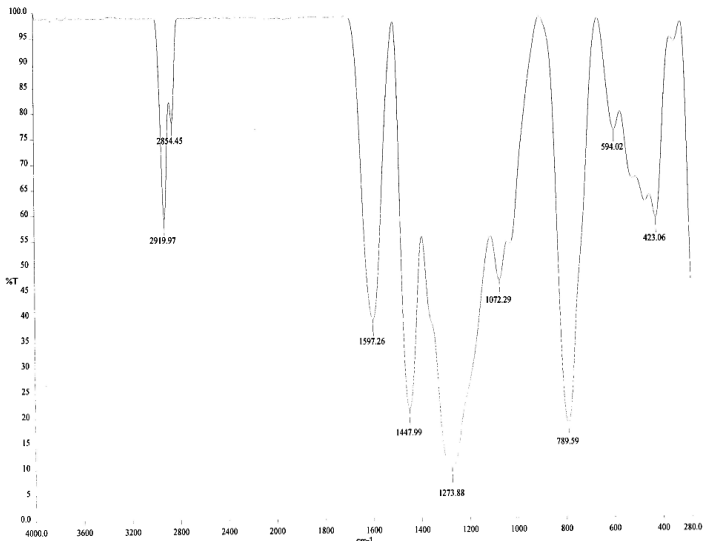

Supplementary Material 14: Ftir Spectrum of Morindone **(4).**

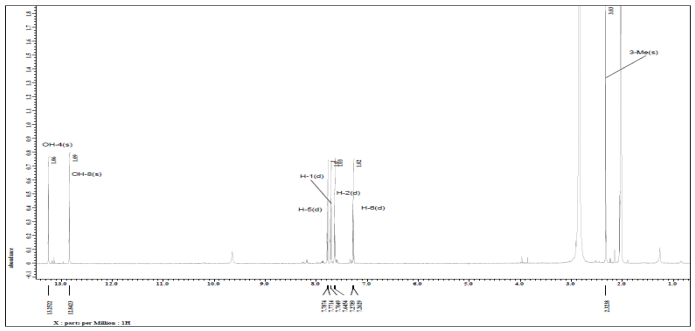

Supplementary Material 15: ^{1}H NMR Spectrum of Morindone **(4).**

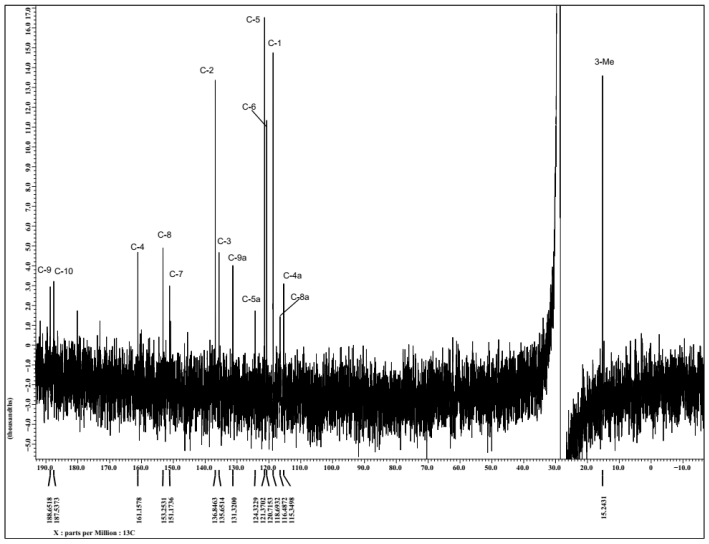

Supplementary Material 16: ^{13}C Nmr Spectrum of Morindone **(4).**

1,6-dihydoxy-5-methoxy-2-methyl anthraquinone (5): Orange yellow amorphous powder ($CHCl_3$); UV (EtOH) λmax 240, 314, 480 nm; IR ν_{max} 2852, 1575, 1359, 1268 and 1026 cm^{-1}; EIMS m/z 284 [M+], 269, 238, 181, 128, 77, 51; ^{1}H and ^{13}C- NMR spectra are consistent with literature [23] (Supplementary Material 17-20).

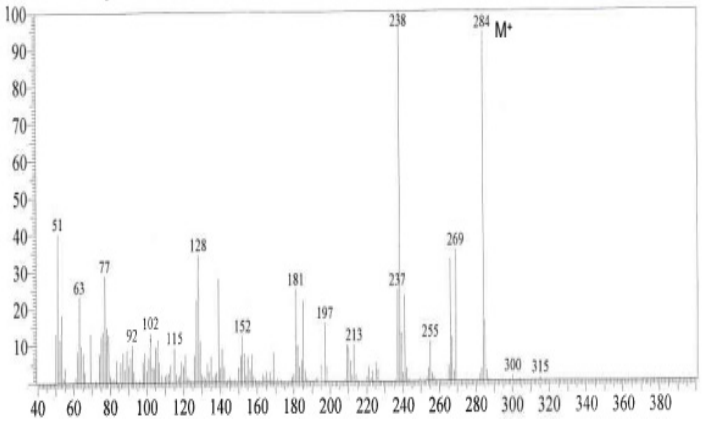

Supplementary Material 17: Eims Spectrum of 1,6-Dihydoxy-5-Methoxy-2-Methyl Antraquinone **(5).**

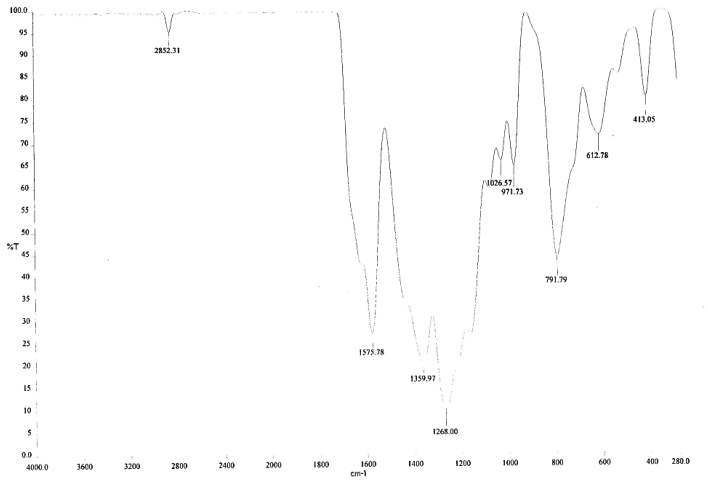

Supplementary Material 18: Ftir Spectrum of 1,6-Dihydoxy-5-Methoxy-2-Methyl Anthraquinone **(5).**

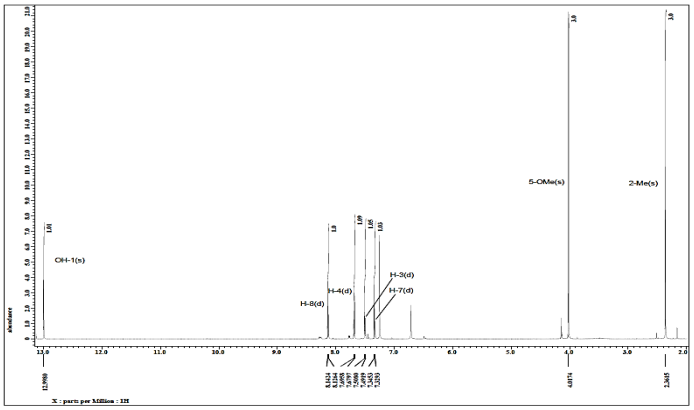

Supplementary Material 19: ^{1}H Nmr Spectrum of 1,6-Dihydoxy-5-Methoxy-2-Methyl Antraquinone (**5**).

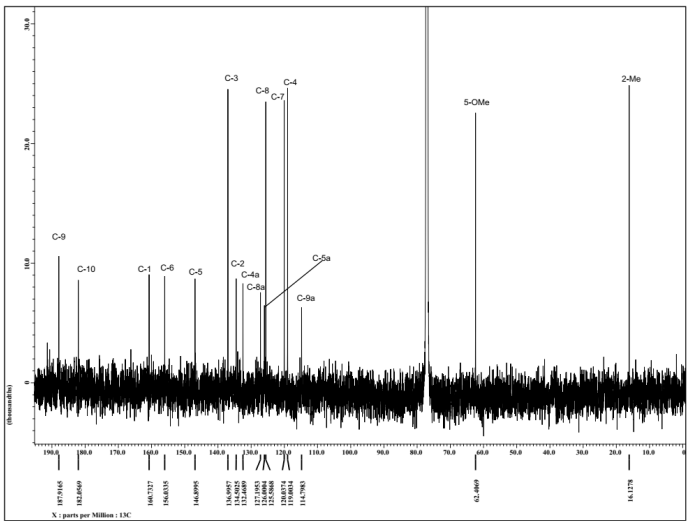

Supplementary Material 20: ^{13}C Nmr Spectrum of 1,6-Dihydoxy-5-Methoxy-2-Methyl Antraquinone **(5).**

Sorendidiol (**6**): Yellow needle crystal (Acetone); m.p. 286-288ºC (literature 287-288ºC, [24]); UV (EtOH) λmax 412 and 320 nm; IR ν_{max} 3295, 2930, 1740, 1561, 1440, 1294 and 1108 cm^{-1}; EIMS m/z 254 [M+], 225, 197, 139, 115; ^{1}H and ^{13}C NMR spectra are consistent with literature [20] (Supplementary Material 21-24.

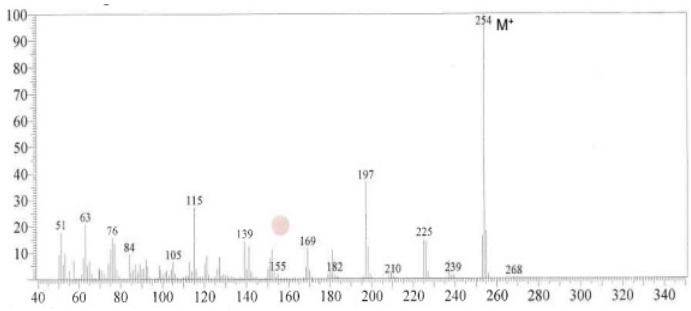

Supplementary Material 21: Eims Spectrum of Sorendidiol (**6**)

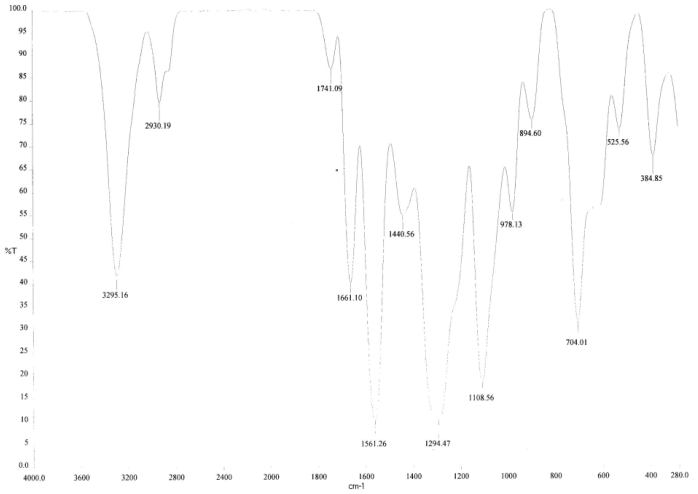

Supplementary Material 22: Ftir Spectrum of Sorendidiol **(6).**

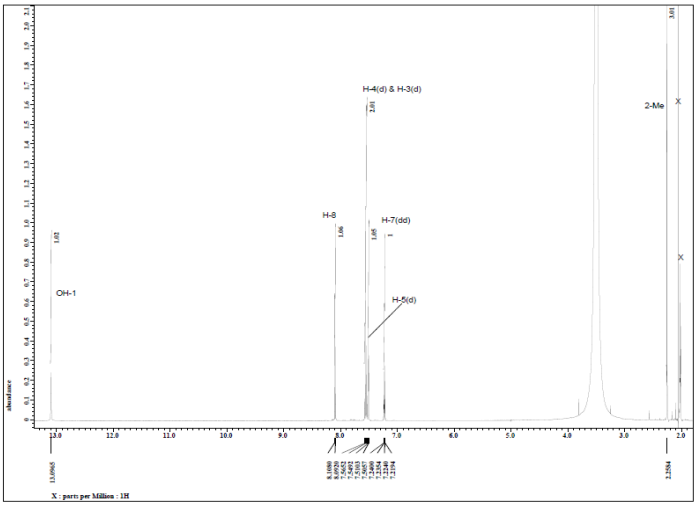

Supplementary Material 23: ^{1}H Nmr Spectrum of Sorendidiol **(6).**

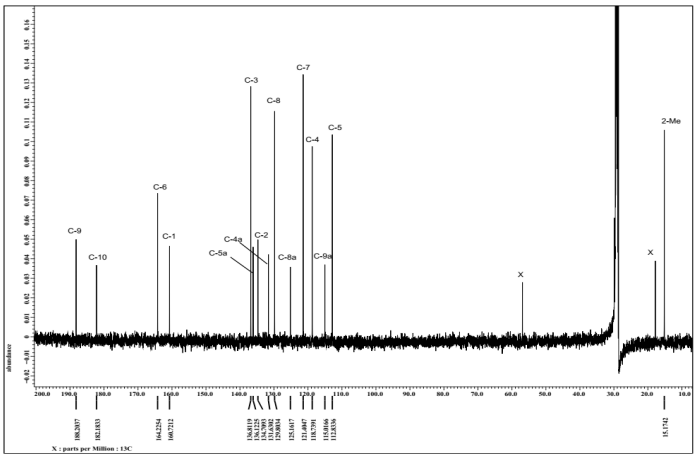

Supplementary Material 24: ^{13}C Nmr Spectrum of Sorendidiol **(6).**

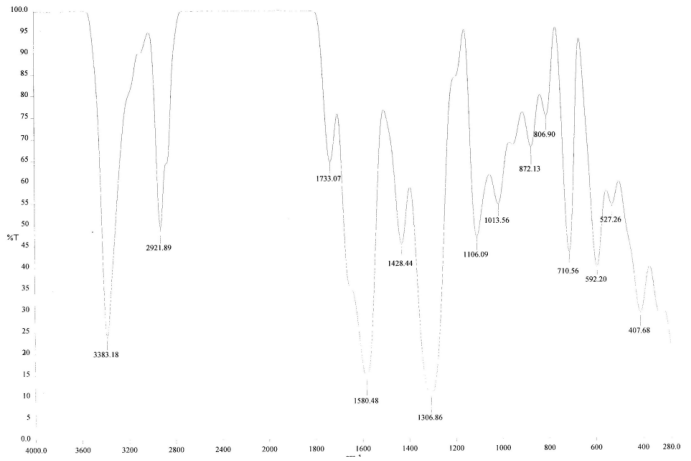

Supplementary Material 26: Ftir Spectrum of Rubiadin **(7).**

Rubiadin (7): Yellow needle crystal (Acetone); m.p. 288-290ºC (literature 290-291ºC, [25]); UV (EtOH) λmax 419, 324 and 225 nm; IR ν_{max} 3383, 2918, 1733, 1580, 1428, 1306 and 1106 cm^{-1}; EIMS m/z 254 [M+], 226, 197, 152, 115, 76; ^{1}H and ^{13}C NMR spectra are consistent with literature [20] (Supplementary Material 25- 28.

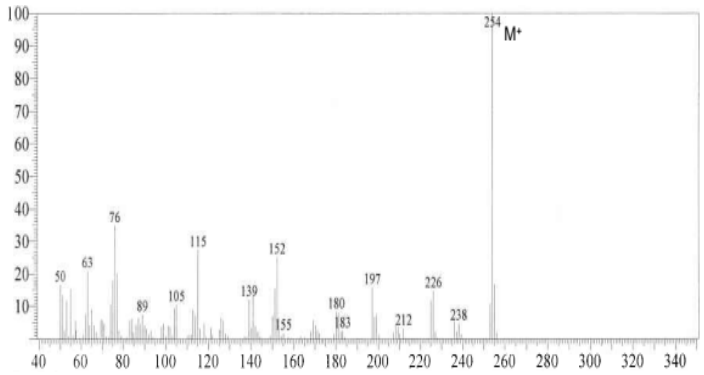

Supplementary Material 25: EIMS Spectrum of Rubiadin (7).

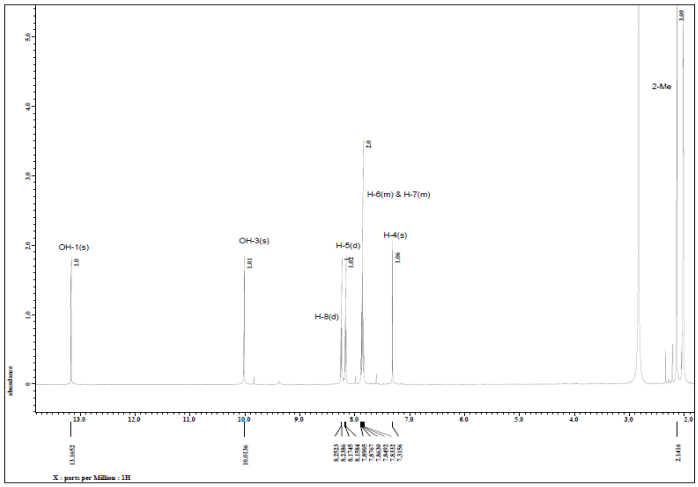

Supplementary Material 27: ^{1}H NMR Spectrum of Rubiadin **(7).**

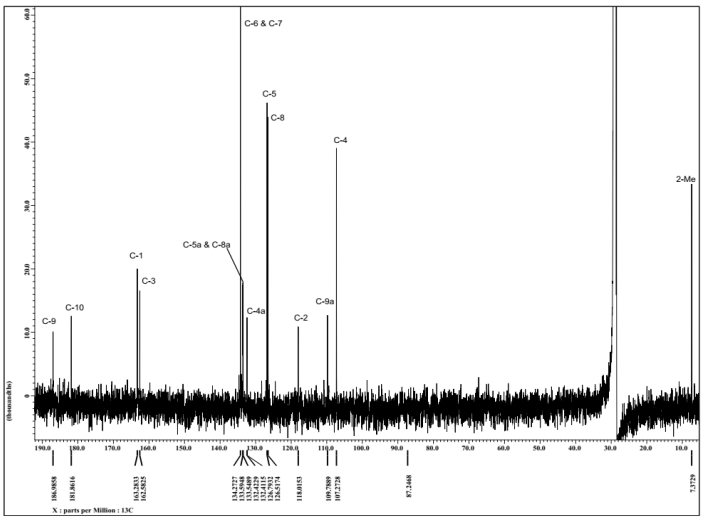

Supplementary Material 28: ^{13}C NMR Spectrum of Rubiadin **(7).**

Alizarin (8): Yellow needle crystal ($CHCl_3$); m.p. 280-284ºC (literature 289ºC); UV (EtOH) λmax 412 and 303 nm; IR ν_{max} 3188, 1928, 1659, 1564, 1447, 1301, 1247 and 1044 cm^{-1}; EIMS m/z 254 [M+], 236, 208, 139, 77; ^{1}H and ^{13}C- NMR spectra are consistent with literature [26] (Supplementary Material 28-31).

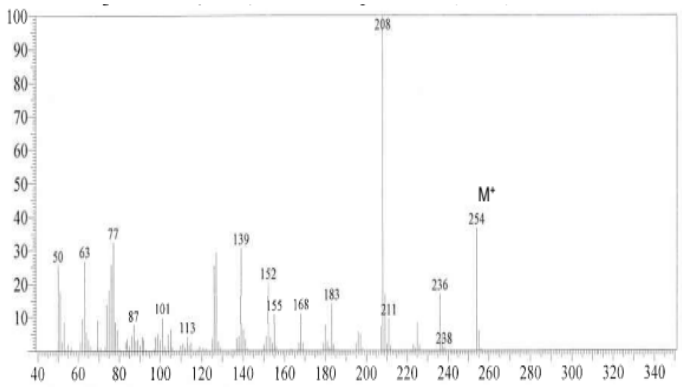

Supplementary Material 29: Eims Spectrum of Alizarin **(8).**

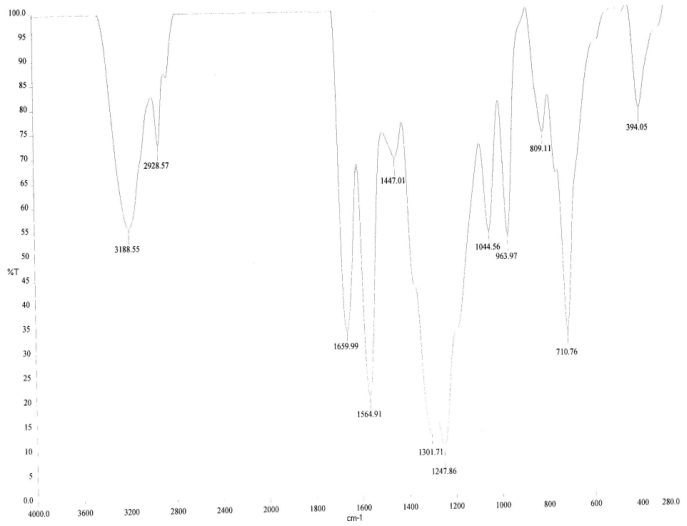

Supplementary Material 30: Ftir Spectrum of Alizarin **(8).**

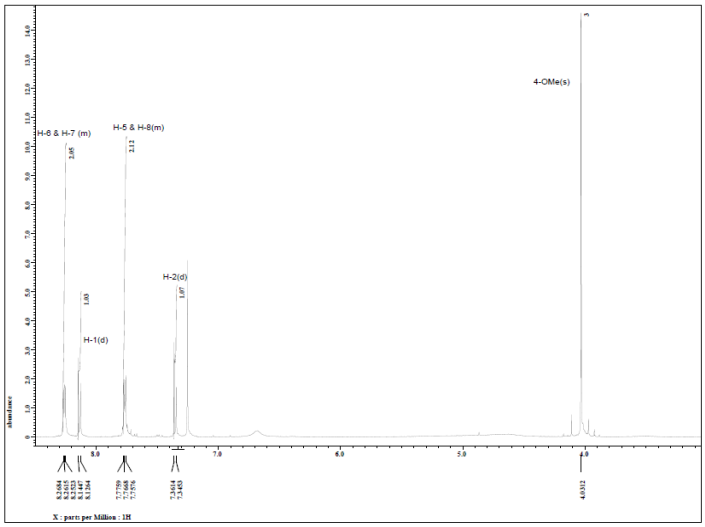

Supplementary Material 31: ^{1}H Nmr Spectrum of Alizarin **(8).**

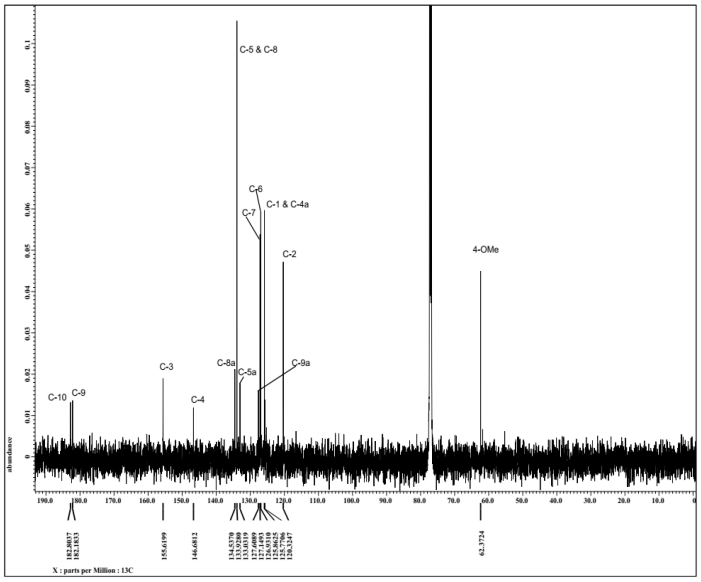

Supplementary Material 32: ^{13}C Nmr Spectrum of Alizarin **(8).**

1,4-dihydroxy-2-methoxy anthraquinone (9): Reddish orange amorphous powder ($CDCl_3$); UV(EtOH) λmax 420 and 312 nm; IR ν_{max} 2921, 2859, 1725, 1454, 1253, 1089 cm^{-1}; EIMS m/z 270 [M+], 227, 143, 87, 74; ^{1}H and ^{13}C- NMR spectra are consistent with literature [27] (Supplementary Material 32-35).

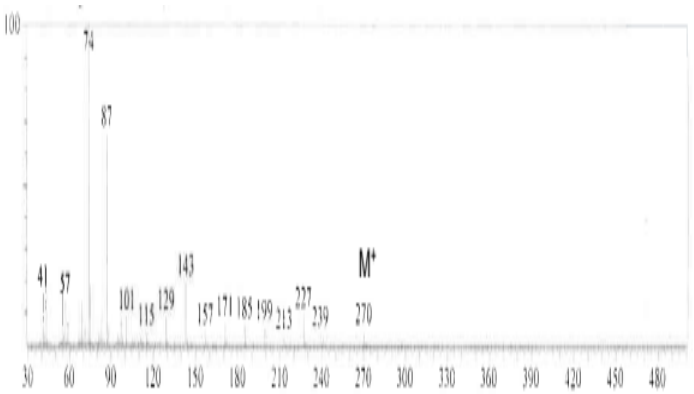

Supplementary Material 33: Eims Spectrum of 1,4-Dihydroxy-2-Methoxy Anthraquinone **(9).**

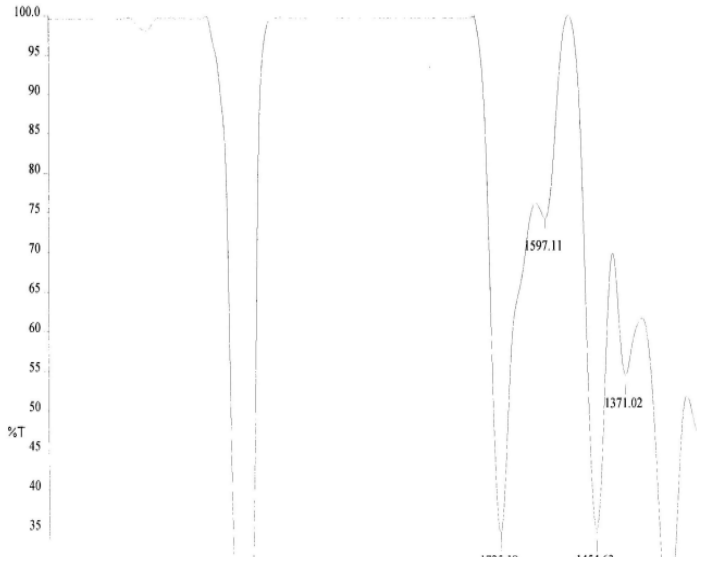

Supplementary Material 34: Ftir Spectrum of 1,4-Dihydroxy-2-Methoxy Anthraquinone **(9).**

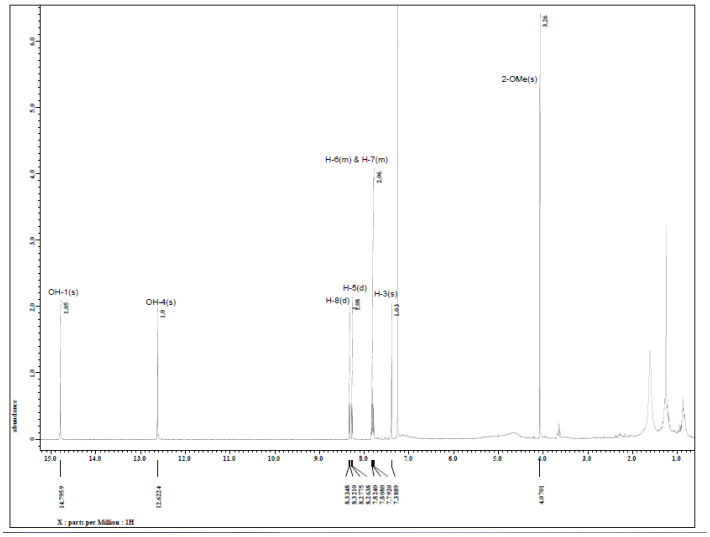

Supplementary Material 35: ^{1}H Nmr Spectrum of 1,4-Dihydroxy-2-Methoxy Anthraquinone **(9).**

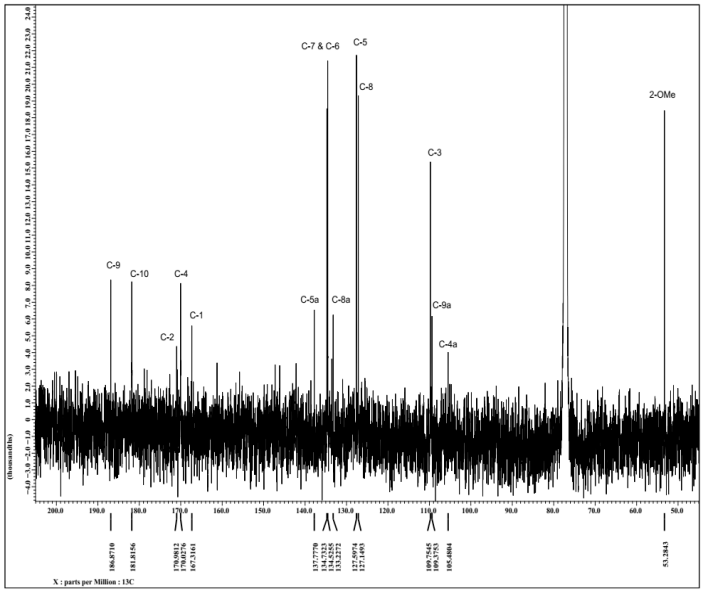

Supplementary Material 36: ^{13}C Nmr Spectrum of 1,4-Dihydroxy-2-Methoxy Anthraquinone **(9)**

Damnacanthol (10): Yellow needle crystal (MeOH); m.p. 156-158ºC (literature 157ºC [21]); UV (EtOH) λmax 427, 282 and 215 nm; IR ν_{max} 3066, 2925, 1653, 1565, 1444, 1339 and 1258 cm^{-1}; EIMS m/z 284 [M+], 269, 251, 237, 181, 152, 139, 76; ^{1}H and ^{13}C-NMR spectra are consistent with literature [21] (Supplementary Material 37-40).

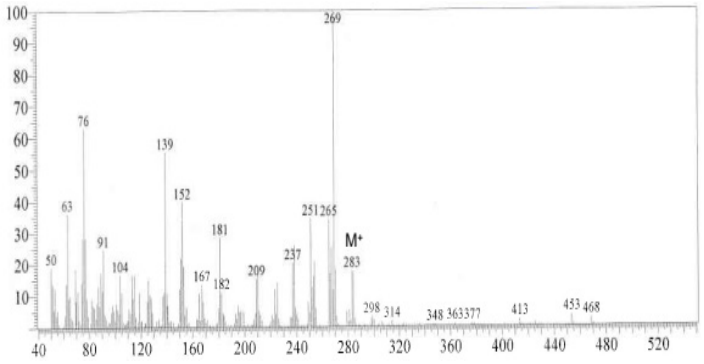

Supplementary Material 37: Eims Spectrum of Damnacanthol **(10).**

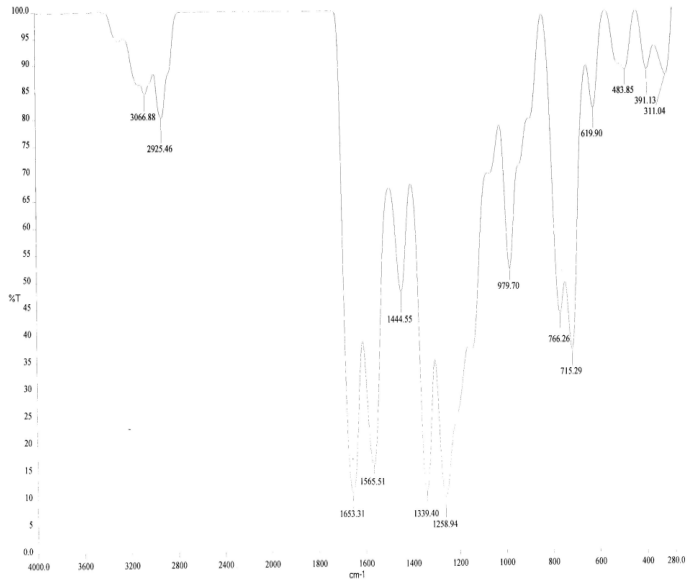

Supplementary Material 38: Ftir Spectrum of Damnacanthol **(10).**

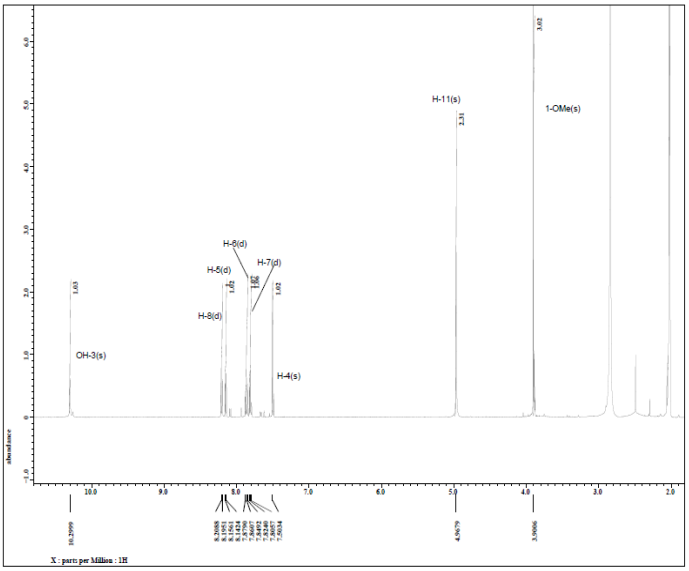

Supplementary Material 39: ^{1}H Nmr Spectrum of Damnacanthol **(10).**

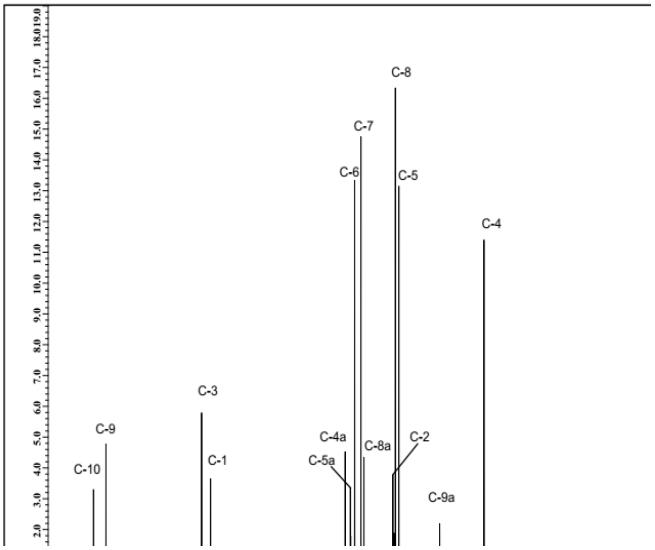

Supplementary Material 40: ^{13}C Nmr Spectrum of 1 Damnacanthol **(10).**

1,3-dihydroxy-2-methoxy anthraquinone (**11**): Yellow needle crystal (MeOH); m.p. 218-220ºC (literature 219-220ºC [28]); UV(EtOH) λmax 411, 245 and 205 nm; IR ν_{max} 3410, 2926, 1639, 1581, 1452, 1382 and 1276 cm^{-1}; EIMS m/z 270 [M+], 252, 227, 196, 115; ^{1}H and ^{13}C- NMR spectra are consistent with literature [28] (Supplementary Material 41-44).

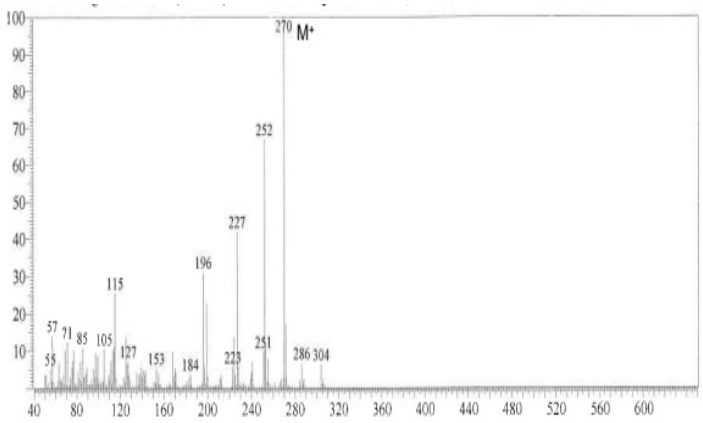

Supplementary Material 41: Eims Spectrum of 1,3-Dihydroxy-2-Methoxy Anthraquinone **(11).**

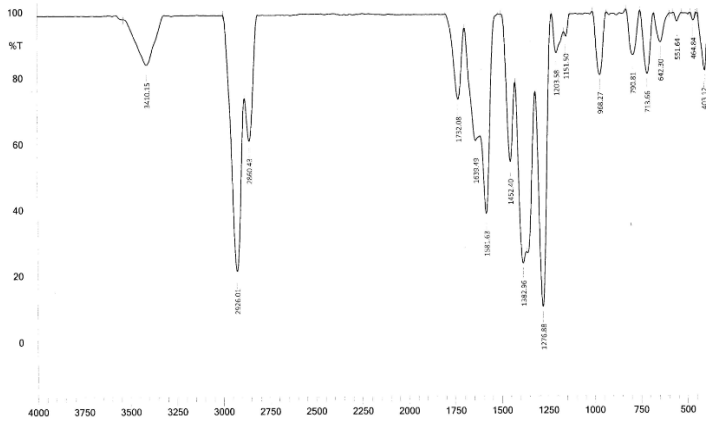

Supplementary Material 42: Ftir Spectrum of 1,3-Dihydroxy-2-Methoxy Anthraquinone **(11).**

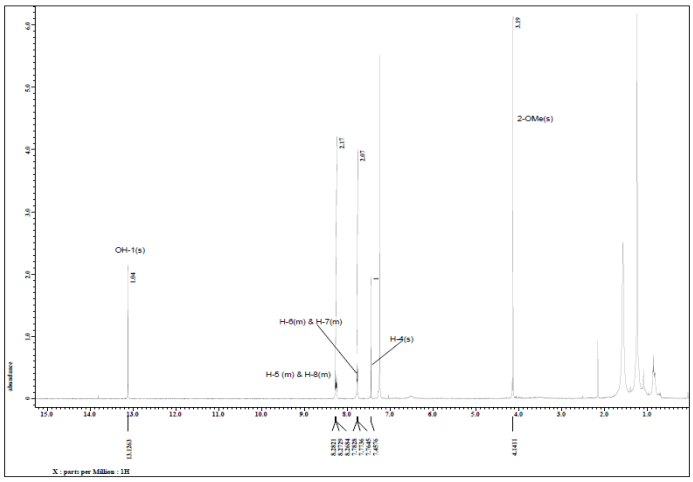

Supplementary Material 43: ^{1}H Nmr Spectrum of 1,3-Dihydroxy-2-Methoxy Anthraquinone **(11).**

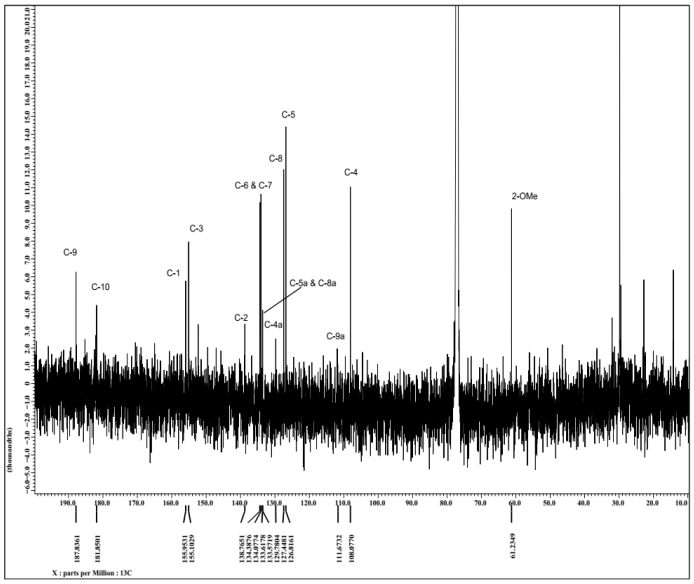

Supplementary Material 44: ^{13}C Nmr Spectrum of 1,3-Dihydroxy-2-Methoxy Anthraquinone **(11).**

Lucidin-ω-methyether (12): Orange-Yellow needle crystal (Acetone); m.p. 170-173ºC (literature 170ºC [29]); UV(EtOH) λmax 419, 325 and 226 nm; IR ν_{max} 3142, 2924, 1672, 1573, 1367, 1332 and 1273 cm-^{1}; EIMS m/z 284 [M+], 252, 196, 168; ^{1}H and ^{13}C- NMR spectra are consistent with literature [29] (Supplementary Material 45-48).

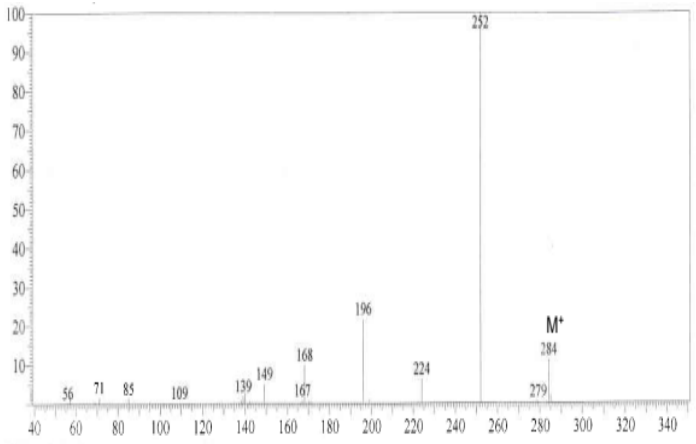

Supplementary Material 45: Eims Spectrum of Lucidin-Ω-Methyether **(12).**

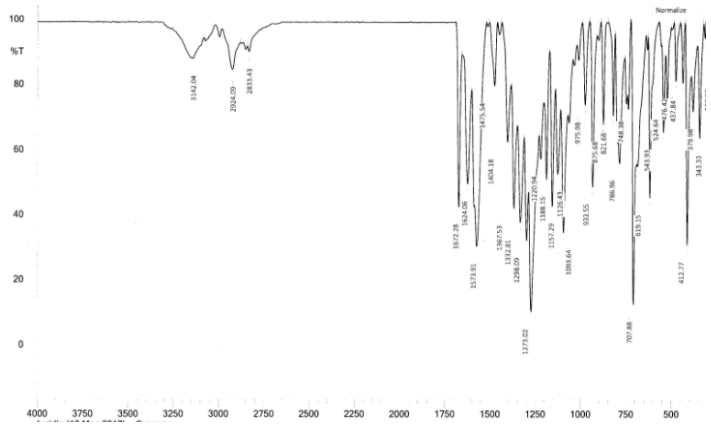

Supplementary Material 46: Ftir Spectrum of Lucidin-Ω-Methylether **(12).**

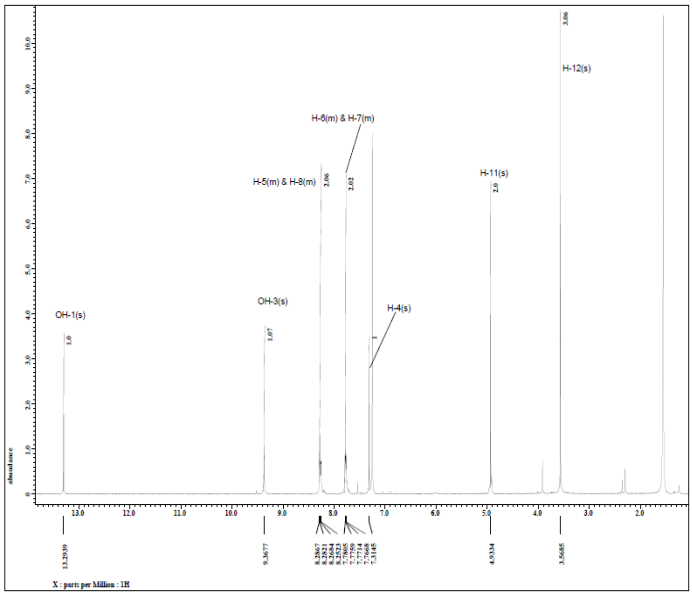

Supplementary Material 47: ^{1}H Nmr Spectrum of Lucidin-Ω-Methyether **(12).**

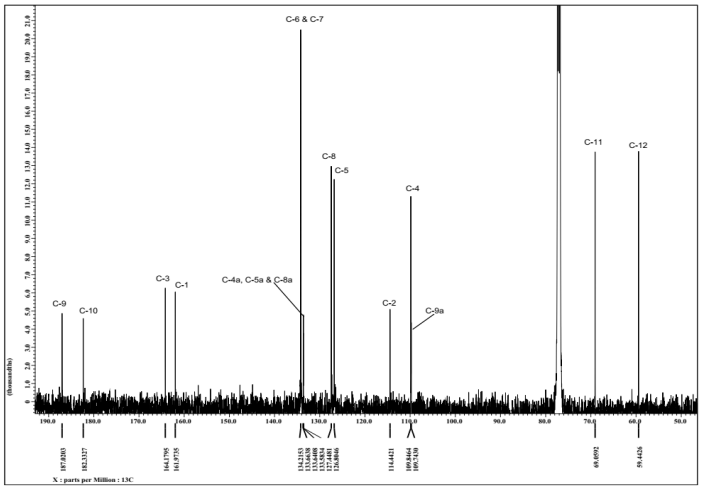

Supplementary Material 48: ^{13}C Nmr Spectrum of Lucidin-Ω-Methyether **(12).**

Cytotoxic Assay

The cytotoxic assays were performed using MTT assay described by Mosmann, 1983. All cell lines for this work were obtained from Taylor's University, Malaysia. The cytotoxicities of the compounds were expressed as IC_{50} values. Cis-diammineplatinum (II) chloride was used as standard compound for all cancer cell lines.

Molecular Docking

The three-dimensional structure of selected ligand was generated and optimized by using MMFF94s force field in Avogadro software [30,31]. The crystal structures of HER-2 (PDB ID: 3PP0, chain A), β-catenin (PDB ID: 1JDH, chain A) and Src protein kinase (PDB ID: 2SRC) receptor proteins were retrieved from the Protein Data Bank (www.rcsb.com). Then, hydrogen atoms were added to the protein structures using Auto Dock Tools [32]. The docking was performed using Auto Dock Vina [33]. The grid box was set to cover important residues involved in ligand binding, Lys435 and Lys312 in β-catenin. Meanwhile, the grid boxes for HER2 and Src kinase were located and identified from the co-crystallized ligand that were bound to the protein receptor in HER2 and Src kinase crystal structures. The dimension of the grid box is tabulated (Table 1).

	Colon cancer (LS174T)		**Stomach cancer (SNU-1)**	**Leukaemia (K562)**
	B-catenin (site A)	B-catenin (site B)		
x-dimension	20	30	20	20
y-dimension	20	30	20	20
y-dimension	20	30	20	20
X centre	-6.485	-0.707	16.387	16.4
Y centre	0.514	11.906	17.394	20.969
Z centre	51.129	21.721	26.218	58.729

Table 1: Docking Parameters.

The grid box spacing was set to be 1.0 angstrom so that all the residues are available in equal-opportunity zone for ligand binding. In β-catenin, two grid boxes were set due to the existence of two active sites (here after named Site A and Side B) which are important for β-catenin and Tcf interaction [34]. Control docking jobs were carried out on each protein receptors. The purpose is to evaluate the reliability of Vina software in reproducing ligand conformation to the ones observed in the crystal structures. For HER2 and Src kinase, the control docking was preformed using respective co-crystallized ligand. Meanwhile, the control docking for β-catenin was performed using isorhamnetin, a ligand that was reported to have biological activity against β-catenin [35]. Isorhamnetin was shown to actively inhibit β-catenin in 24 hours at 5 μM [36]. The docked complex of compound with the protein receptor was carefully inspected and analyzed using LIGPLOT [37].

Statistical Analysis

The cytotoxicity test data were represented as mean with standard errors obtained from three independent experiments, in which each experiment was performed in triplicate. The graphs were generated using Microsoft Excel Software (Version 2010). The independent sample T-test was performed by SPSS 14.0 to determine significant difference between the sample and standard drug, *cis*-diammineplatinum (II) chloride. The significance level was set at $p < 0.05$.

Results and Discussions

Cytotoxic Activity Evaluation

In this study, a total of twelve anthraquinones isolated from *Morinda citrifolia* were screened for cytotoxic activities against SNU-1, LS-174T and K562 cells. The structure-activity relationships of these anthraquinone were studied to predict the influence of substituent groups towards cytotoxicity. The general chemical structures of the anthraquinones consist of three rings with two carbonyl groups attached to the middle ring. This carbonyl group can play a role as hydrogen acceptor which is important for cytotoxic activities [38]. Theoretically, the hydrogen bonds that are formed between the compound and mutated protein in the cancer cell will increase the cytotoxic activities. *Cis*-diammineplatinum (II) chloride was used as standard drug for all cancer cells. It is a well-known synthetic inorganic drug used as a chemotherapeutic in the treatment of ovarian, testicular, head and neck carcinomas [39]. From the literature, *cis*-diammineplatinum (II) chloride

showed a strong activity towards those cell lines [40,41]. The IC_{50} values of all twelve compounds and the standard compound are tabulated (Table 2) (Supplementary Material 49-76).

Compound	**IC_{50} (µg/ml)**		
	SNU-1	LS-174T	K562
Nordamnacanthal (**1**)	11.26±0.37	3.41 ± 0.21*	5.99±0.41*
Damnacanthal (**2**)	5.52±0.16*	3.86 ± 0.07*	11.15±0.57*
1,3,5-trihydoxy-2-methoxy-6-methyl antraquinone (**3**)	13.10±0.07*	15.88 ± 0.97*	>50
Morindone (**4**)	2.72 ± 0.05*	2.93 ± 0.15*	16.24±0.34*
1,6-dihydoxy-5-methoxy-2-methyl antraquinone (**5**)	>50	19.11±2.41*	>50
Sorendidiol (**6**)	>50	>50	>50
Rubiadin (**7**)	>50	>50	>50
Alizarin (**8**)	>50	>50	>50
1,4-dihydroxy-2-methoxy antraquinone(**9**)	>50	>50	>50
Damnacanthol (**10**)	>50	4.81±0.21*	9.16±0.32*
1,3-dihydroxy-2-methoxy antraquinone (**11**)	>50	>50	>50
Lucidin-ω-methylether (**12**)	26.54± 0.05*	13.28 ± 0.83*	>50
cis- diammineplatinum (II) chloride	9.64 ± 0.59	1.32 ± 0.03	4.08±0.09
The (*) symbol denotes significant difference between sample and positive control, *cis*-diammineplatinum (II) chloride ($p<0.05$).			

Table 2: Cytotoxic activities of compounds **1-12** towards SNU-1 cell line (stomach cancer) LS-174T cell line (colon cancer and K562 (leukemia).

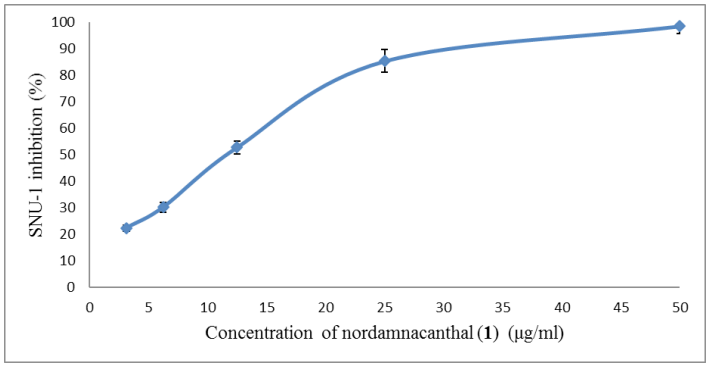

Supplementary Material 49: Cytotoxic activity for nordamnacanthal **(1)** toward SNU-1 (stomach cancer).

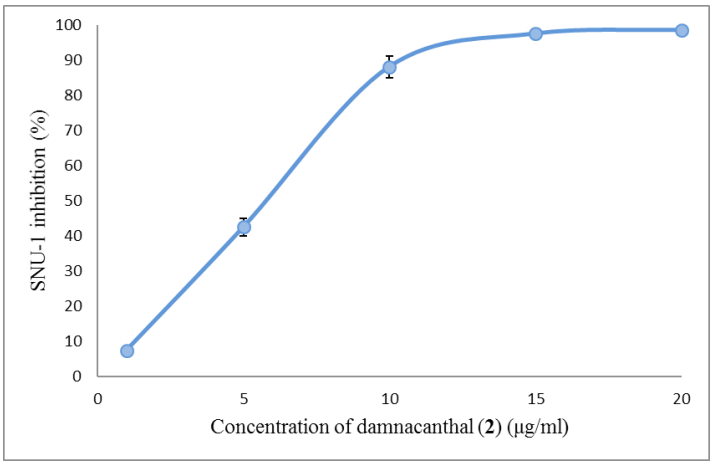

Supplementary Material 50: Cytotoxic activity for damnacanthal (**2**) toward SNU-1 (stomach cancer).

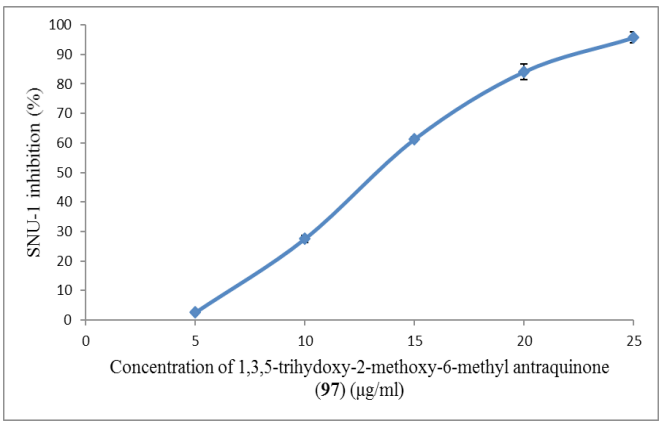

Supplementary Material 51: Cytotoxic activity for 1,3,5-trihydoxy-2-methoxy-6-methyl antraquinone **(3)** toward SNU-1 (stomach cancer).

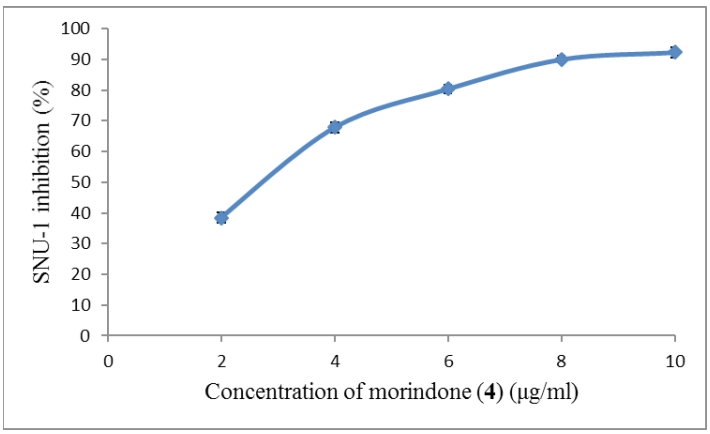

Supplementary Material 52: Cytotoxic activity for morindone (**4**) toward SNU-1 (stomach cancer).

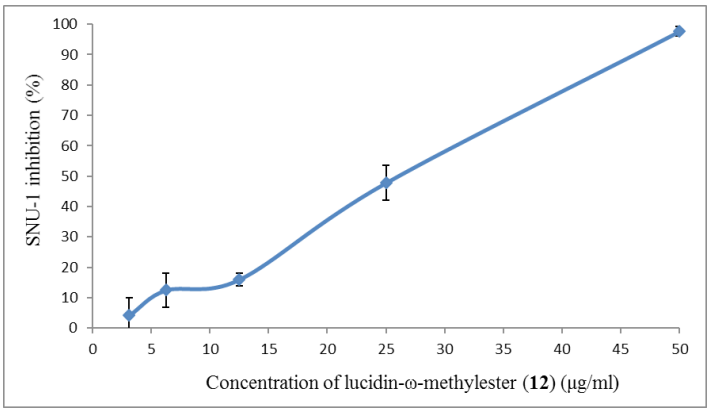

Supplementary Material 53: Cytotoxic activity for lucidin-ω-methylether **(12)** toward SNU-1 (stomach cancer).

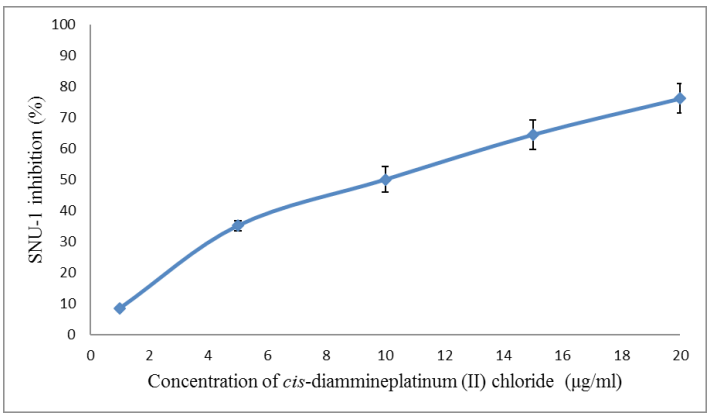

Supplementary Material 54: Cytotoxic activity for standard drug *cis*-diammineplatinum (II) chloride toward SNU-1 (stomach cancer).

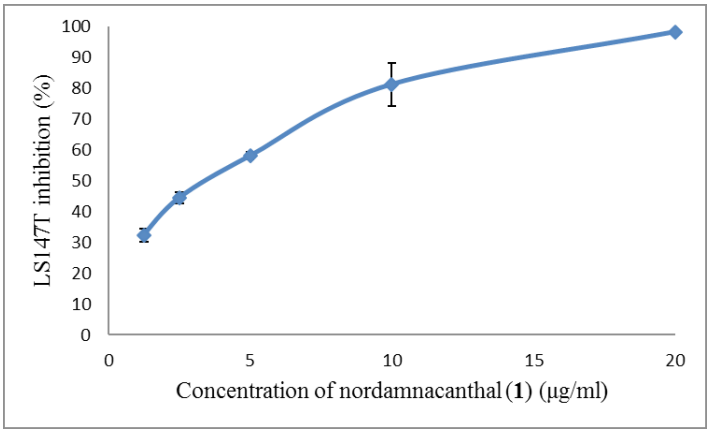

Supplementary Material 55: Cytotoxic activity for the nordamnacanthal **(1)** toward LS174T (colon cancer).

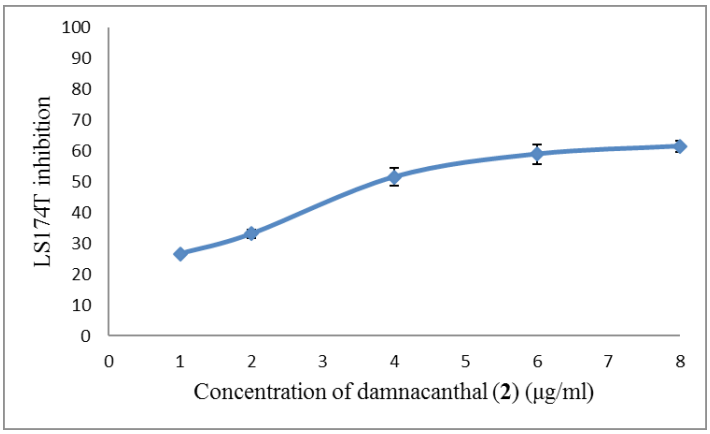

Supplementary Material 56: Cytotoxic activity for the damnacanthal **(2)** toward LS174T (colon cancer).

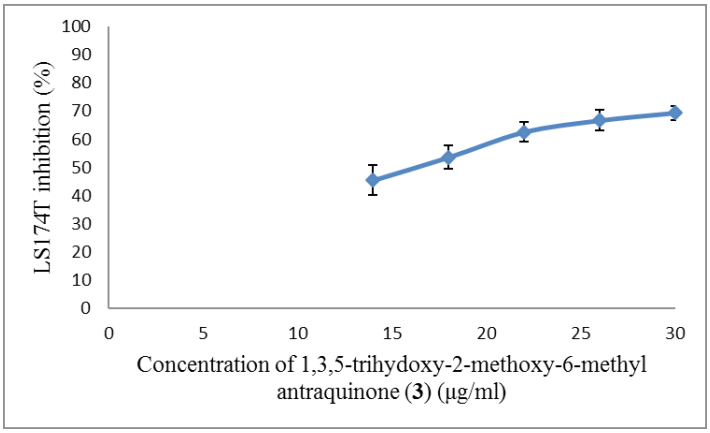

Supplementary Material 57: Cytotoxic activity for the 1,3,5-trihydoxy-2-methoxy-6-methyl antraquinone **(3)** toward LS174T (colon cancer).

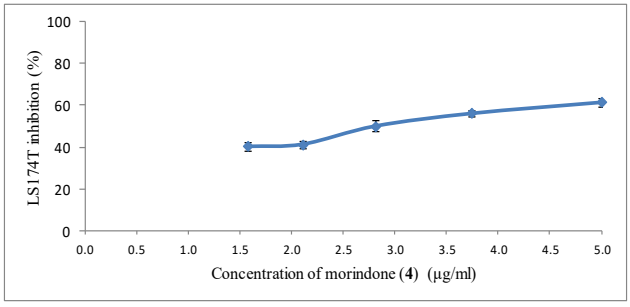

Supplementary Material 58: Cytotoxic activity for the morindone **(4)** toward LS174T (colon cancer).

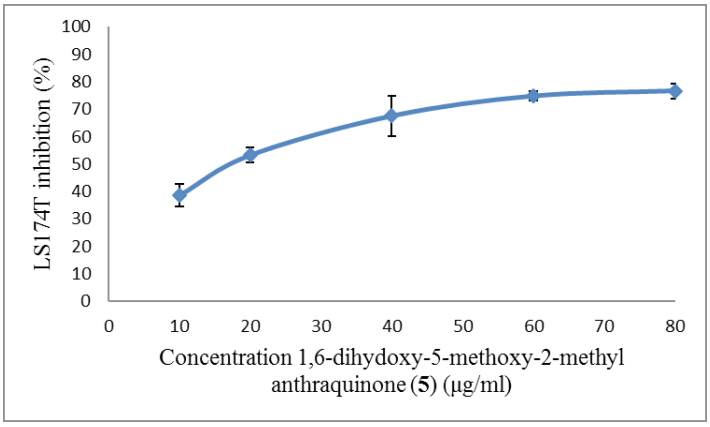

Supplementary Material 59: Cytotoxic activity for the 1,6-dihydoxy-5-methoxy-2methyl anthraquinone **(5)** toward LS174T (colon cancer).

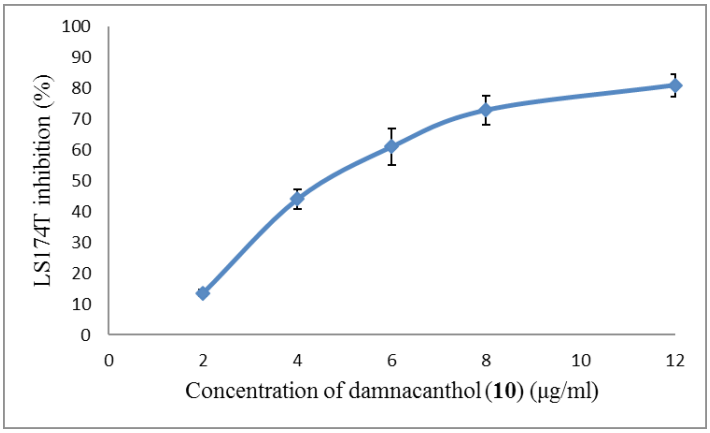

Supplementary Material 60: Cytotoxic activity for the damnacanthol **(10)** toward LS174T (colon cancer).

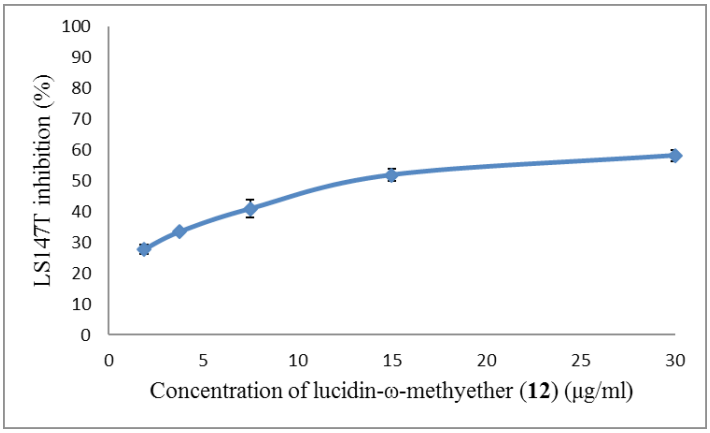

Supplementary Material 61: Cytotoxic activity for the lucidin-ω-methyether **(12)** toward LS174T (colon cancer).

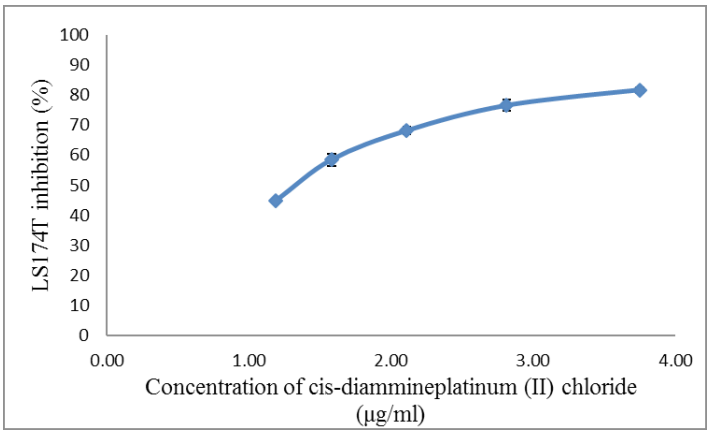

Supplementary Material 62: Cytotoxic activity for the *cis*-diammineplatinum (II) chloride toward LS174T (colon cancer).

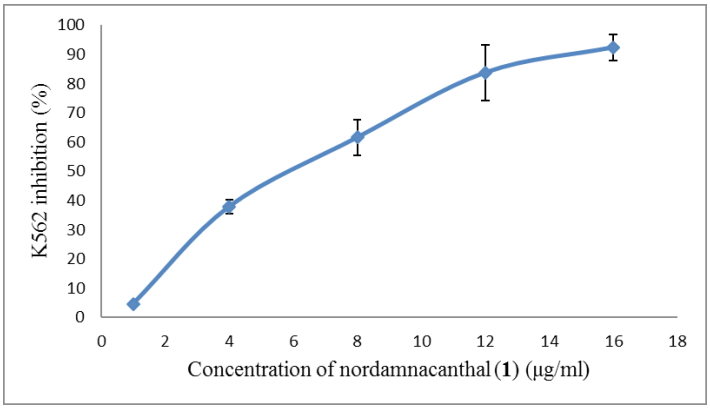

Supplementary Material 63: Cytotoxic activity for the nordamnacanthal **(1)** toward K562 (leukemia).

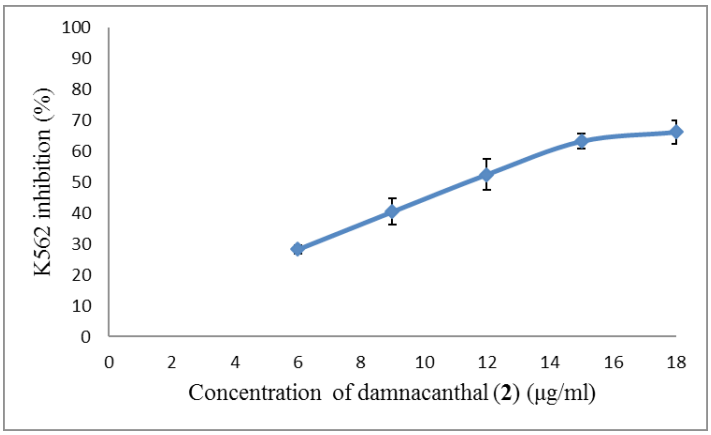

Supplementary Material 64: Cytotoxic activity for the damnacanthal **(2)** toward K562 (leukemia).

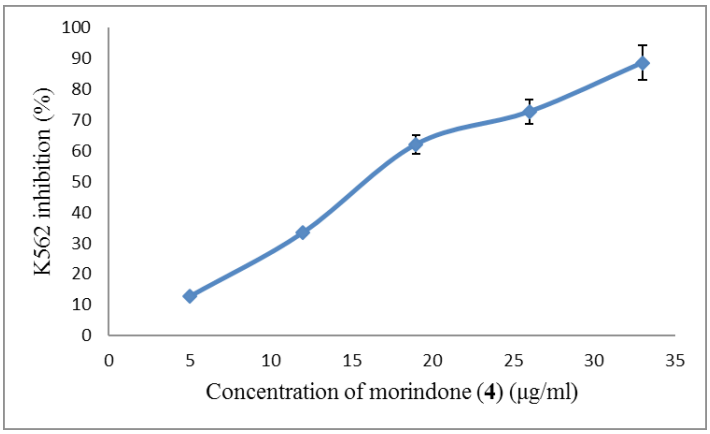

Supplementary Material 65: Cytotoxic activity for the morindone **(4)** toward K562 (leukemia).

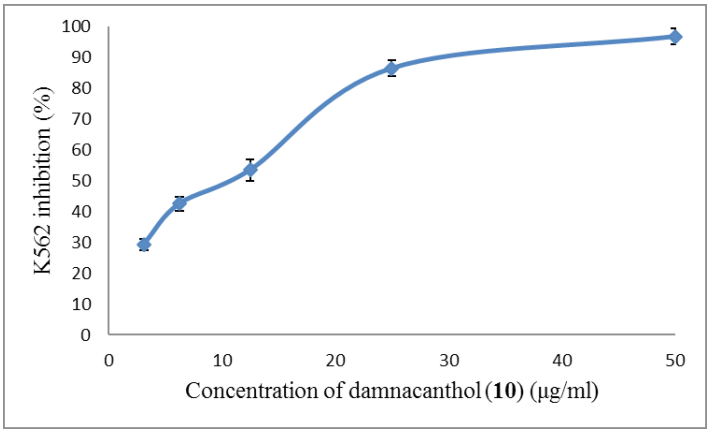

Supplementary Material 66: Cytotoxic activity for the damnacanthol **(10)** toward K562 (leukemia).

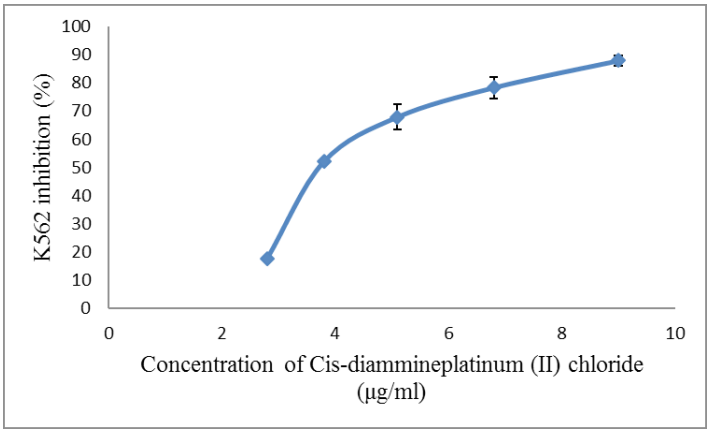

Supplementary Material 67: Cytotoxic activity for the *cis-diammineplatinum* (II) chloride toward K562 (leukemia).

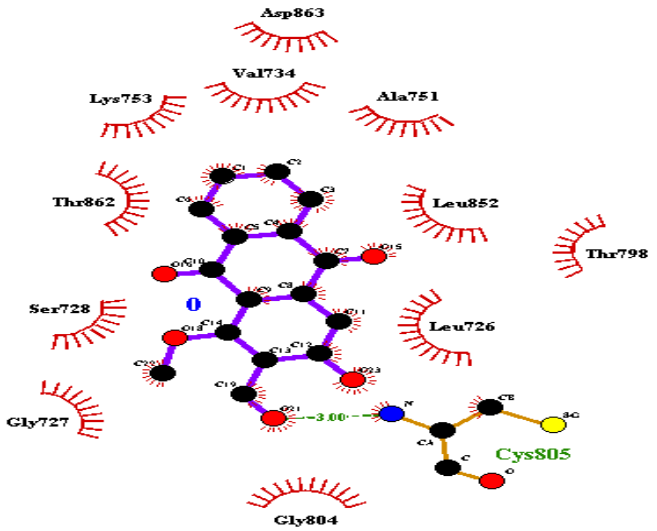

Supplementary Material 68: The interaction forces between damnacanthal **(2)** with HER2 protein in stomach cancer SNU-1.

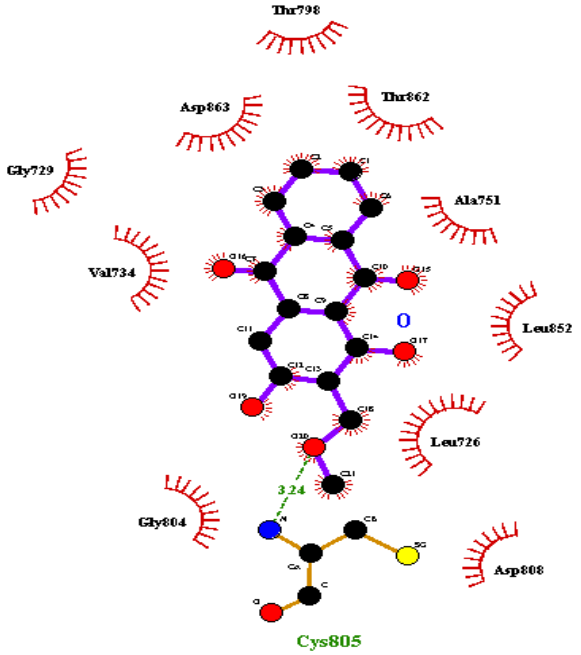

Supplementary Material 69: The interaction forces between Lucidin-ω-methyether **(12)** with HER2 protein in stomach cancer SNU-1.

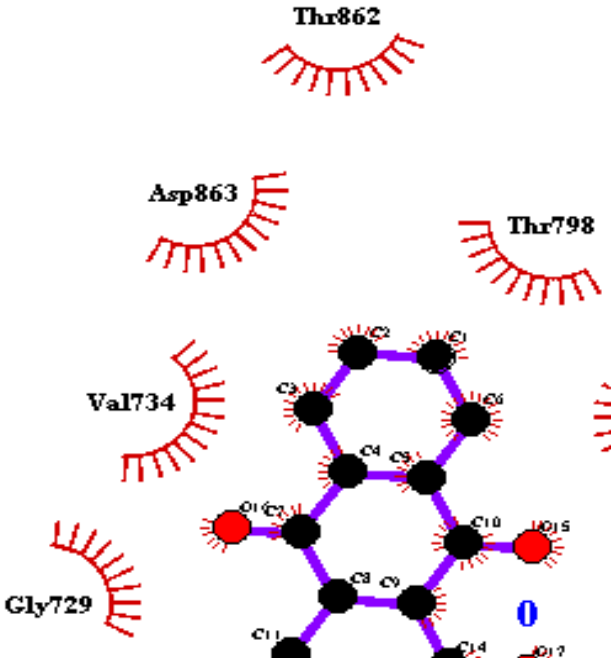

Supplementary Material 69: The interaction forces between nordamnacathal **(1)** with HER2 protein in stomach cancer SNU-1.

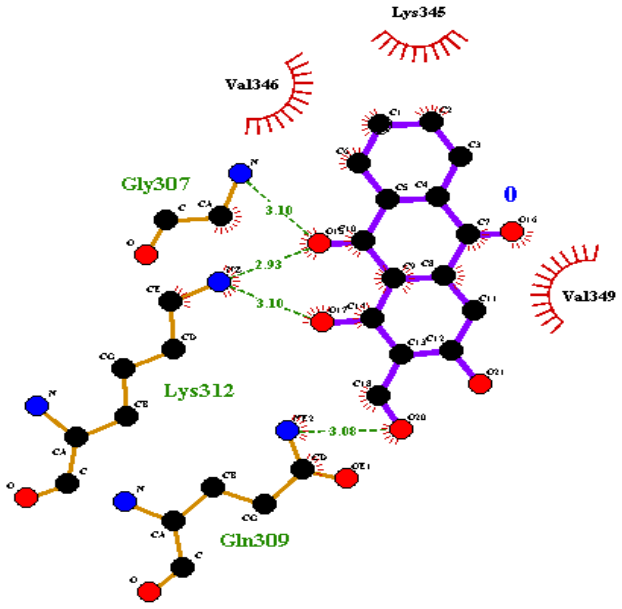

Supplementary Material 71: The interaction forces between nordamnacanthal **(1)** with β-catenin in colon cancer LS174T in active site A.

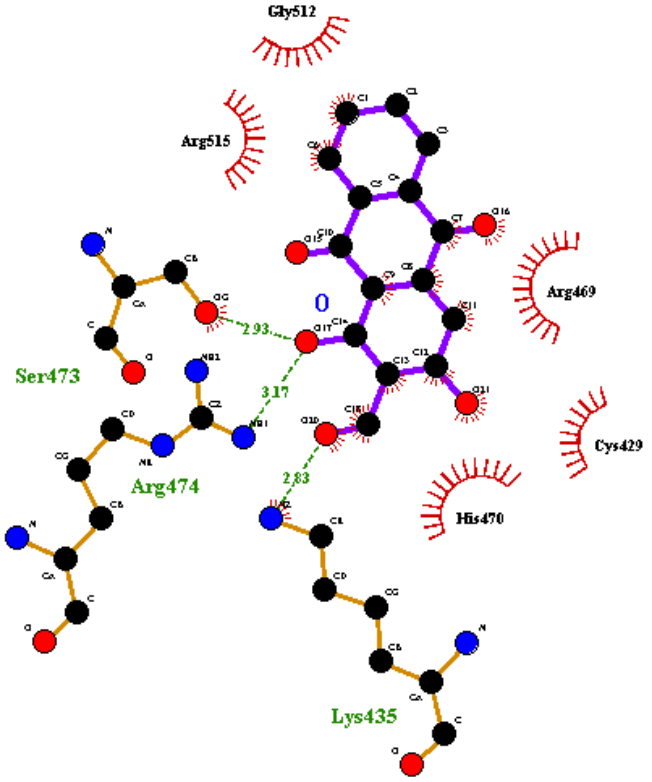

Supplementary Material 72: The interaction forces between nordamnacanthal **(1)** with β-catenin in colon cancer LS174T in active site B.

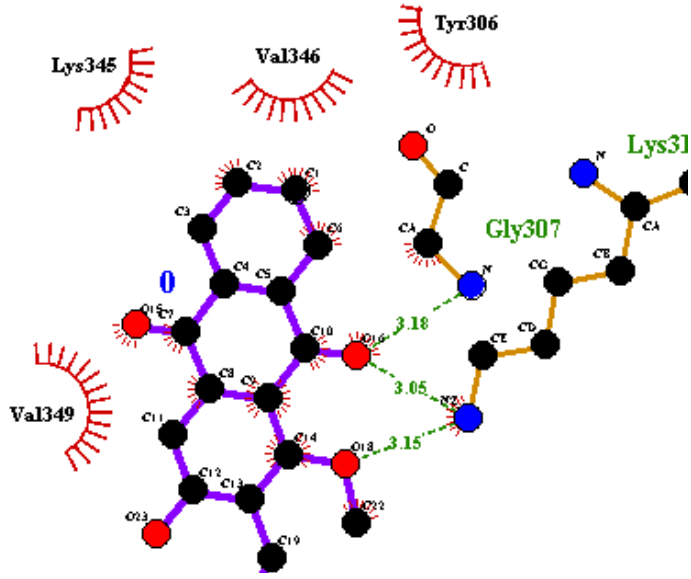

Supplementary Material 73: The interaction forces between damnacanthal **(2)** with β-catenin in colon cancer LS174T in active site A.

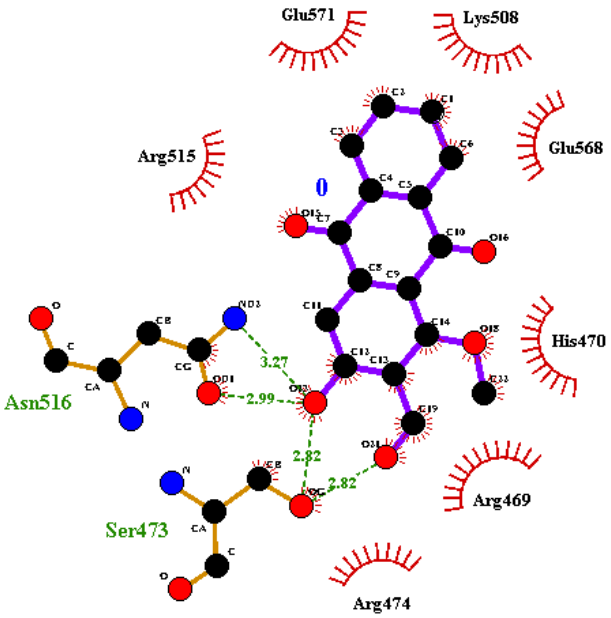

Supplementary Material 74: The interaction forces between damnacanthal **(2)** with β-catenin in colon cancer LS174T in active site B.

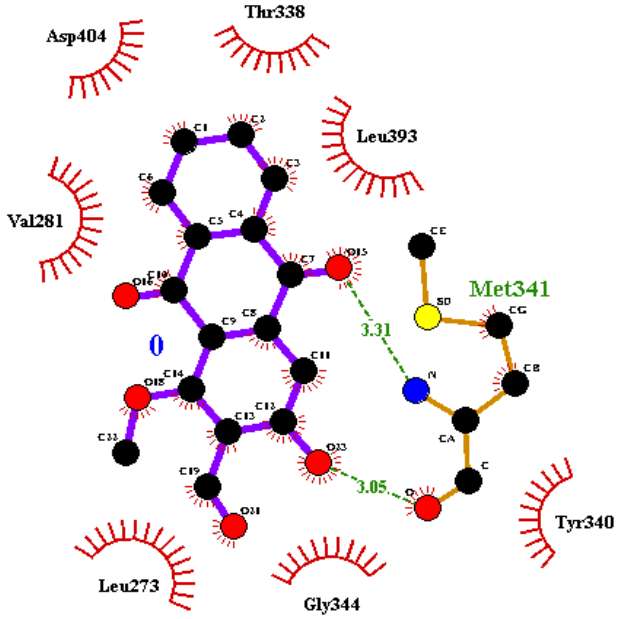

Supplementary Material 75: The interaction forces between damnacanthal **(2)** with Src protein kinase in leukaemia K562 at active activation loop.

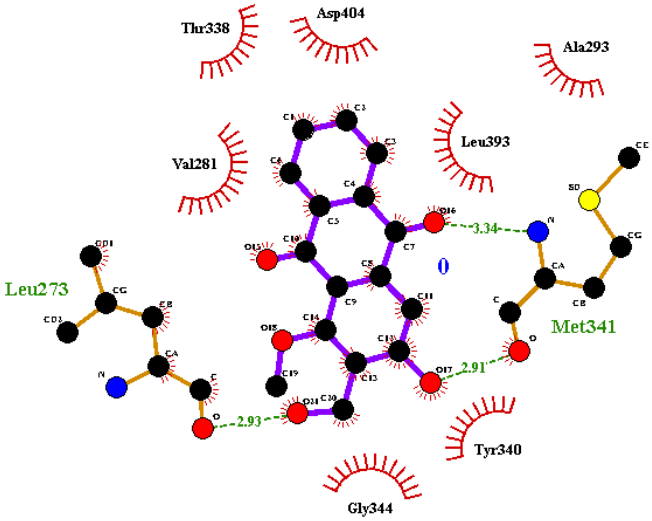

Supplementary Material 76: The interaction forces between damnacanthol **(10)** and leukaemia K562 in activation loop.

The structure-activity relationships on all the tested anthraquinones showed a close correlation between the substituents in the compounds and the cytotoxic activities against SNU-1 cell (Figure 1). An example can be observed in damnacanthal (**2**), which gave a higher cytotoxic activity compared to nordamnacanthal (**1**) due to the presence of methoxyl at C-1. Meanwhile, nordamnacanthal (**1**) and lucidin-ω-methylether (**12**) with almost similar structures to damnacanthal (**2**) showed moderate cytotoxic activities towards SNU-1. This is due to the presence of a hydroxyl group at C-1 for nordamnacanthal (**1**) and methoxyl methyl at C-2 for lucidin-ω-methylether (**12**). Explicitly, morindone (**4**) showed good cytotoxicity against SNU-1 due to the chelated hydroxyl present at two different heterocyclic rings. Previous studies have shown that the presence of two chelated hydrogens at different rings induced DNA damage and apoptosis in SNU-1 by triggered bax pathway [42].

The chemical structures of the twelve derivatives of anthraquinones (Figure 1) were also analyzed for their cytotoxicity against LS174T cell. Among all the tested anthraquinone compounds, morindone (**4**) showed the best cytotoxicity against LS174T cell line. This can be attributed to the presence of two chelated hydroxyl groups in different rings which increases the interaction with the cancer cell. This compound was also reported for having a good inhibition towards Raji cell [43]. Meanwhile, the attachment of two chelated hydroxyl groups in one ring of anthraquinones such as 1, 4-dihydroxy-2-methoxy anthraquinone (**9**) was observed to reduce the cytotoxic activity against LS174T cells. The presence of hydroxymethyl and methoxymethyl at position 2 increases the activity towards LS174T cell in damnacanthol (**10**) and lucidin-ω-methylether (**12**) respectively. This may be due to the binding interaction between the substituents with the amino acid of protein receptor [44]. Both nordamnacanthal (**1**) and damnacanthal (**2**) which contain a formyl moiety at C-2 showed strong cytotoxic activities in the LS-174T cell assay. This suggests that the presence of formyl group at position C2 is necessary for cytotoxic activity. The mild cytotoxic activities observed in 1,3,5-trihydoxy-2-methoxy-6-methyl anthraquinone (**3**) and 1,6-dihydoxy-5-methoxy-2-methyl anthraquinone (**5**) were due to the presence of hydroxyl, methoxyl and methyl substituents in the anthraquinone skeleton.

Among all the anthraquinones, nordamnacanthal (**1**) gave the highest cytotoxic activity against K562 cell line with IC_{50} value of 1.23μg/ml. Unfortunately, compound **1** showed less cytotoxic activity than the standard drug, cis-diammineplatinum (II) chloride. Besides compound **1**, compound **9** also showed good cytotoxic activity towards K562 cell line. Meanwhile, the remaining anthraquinones compounds showed moderate or weak activity against K562 cell line, as listed in (Table 2). Five out of twelve anthraquinones isolated from this species shown cytotoxic activity against K562 cell line. The structure-activity relationships on all the tested anthraquinones showed a close correlation between the substituents existing in the compounds and the cytotoxic activity against SNU-1 cell (Figure 1). The presence of a formyl or a hydroxymethyl group at C-2 in nordamnacanthal (**1**) and damnacanthol (**10**) respectively, gave strong cytotoxic activities against K562 cell line. Meanwhile, damnacanthal (**2**) was cytotoxic due to the presence of a formyl group but it was less active when compared with nordamnacanthal (**1**). Damnacanthal (**2**) has a methoxyl group attached to C-1 instead of a hydroxyl group. Previous studies have shown that the presence of formyl group at C-2 in the anthraquinone skeleton will enhance cytotoxicity in cancer cell lines [43].

Molecular Docking Studies

Molecular docking experiments were carried out to determine the interaction between isolated compounds and the targeted protein receptor in each cancer cell line to support the relationship between chemical structure and bioactivity. This was obtained by generating an interaction model between the ligand and the targeted protein. This binding model derived from a molecular docking experiment was used to understand the anticancer mechanism at molecular level. Prior to this study, a manual inspection of the docked protein-ligand complex was performed rather than selecting the docked complex with the highest binding energy in each molecular docking experiment. The relevance is to provide a rational docked complex that agrees with the IC_{50} value possessed by each ligand. According to Yuen [45], the docked complex with the lowest binding energy does not always represent the true binding of ligand in the biological system. The 2-fold difference in docking score can exist in the face of a large range of IC_{50} value [46]. The ability of a ligand to dock at a binding pocket of a protein is depending on its chemical structure. Among all the twelve isolated anthraquinones tested, morindone (**4**) showed the highest inhibition against SNU-1 cell line and was selected for molecular docking studies. In order to create a binding model between morindone (**4**) and the ATP binding site of HER2 protein,

a molecular docking was performed using the crystal structure of HER2 dimer (PDB: 3PP0). A visual inspection using LIGPLOT analysis (Figure 2) revealed the important binding interactions existing between compound **4** and residues at the ATP binding site of HER2.

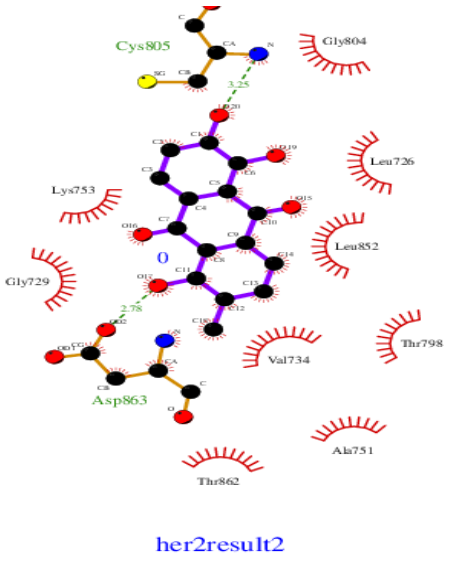

Figure 2: Two-dimensional diagram of binding interaction of the docked structure of morindone (**4**) with HER2 (PDB ID: 3PP0) protein receptor using LIGPLOT [37].

There were two hydrogen bonds between compound 4 and Cys805 and Asp863 with lengths of 3.25Å and 2.78Å, respectively. Morindone (**4**) also interacted through hydrophobic contact with another important amino acid of HER2, Lys753. Other hydrophobic interactions also existed between morindone (**4**) and other residues such as Gly804, Leu726, Leu852, Thr798, Val734, Ala751, Thr862 and Gly729 in the ATP binding sites. The binding interaction of docked HER2-morindone (**4**) complex was compared to that in the HER2-known inhibitor complex (Figure 3).

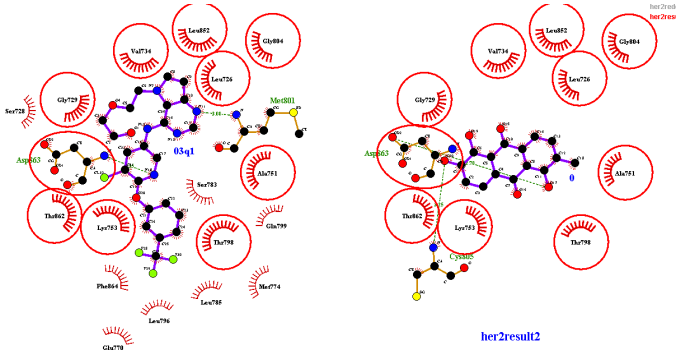

Figure 3: The interaction forces in binding site between known inhibitor (left) and morindone **(4)** (right) with HER2 protein in stomach cancer SNU-1. The common residues are circled.

This is due to morindone (**4**) giving the highest inhibition activity against SNU-1 cell line compared to the other anthraquinones. The observation showed similar hydrophobic contact and one hydrogen bond with Asp863 residue was formed in both complex, explaining the high inhibition activity of morindone (**4**) against SNU-1 cell line. Meanwhile, a formyl moiety present in damnacanthal (**2**) and also in nordamnacanthal (**1**) at position C-2 gave hydrogen bonds with Cys805 with length of 3.00 Å and 2.94 Å respectively. Meanwhile, lucidin-ω-methyether (**12**) which had a methoxyl moiety at C-2 formed a hydrogen bond with Cys805 (3.24 Å). Damnacanthal (**2**) had a high cytotoxic activity compared to nordamnacanthal (**1**) and lucidin-ω-methyether (**12**) because of a hydrophobic interaction with the important amino acid Lys753. The LIGPLOT analyses for these compounds are shown in the supporting material.

In colon cancer, the Wnt/β-catenin/Tcf signalling pathway plays an important role in cancer proliferation and self-renew. An alternative way to modify the signalling is by disrupting the interaction between two proteins along this pathway: β-catenin and Tcf4. There are two active sites (named as Site A and Site B) on β-catenin. Site A of β-catenin contains the key important amino acid Lys312, while Site B contains amino acid Lys435 which are important in the interaction between the protein and the TCF4 protein [47]. Ideally, a potential lead compound to inhibit the proliferation and self-renew process should be able to bind to these important residues and consequently block the active site. An analysis on the docked complex of morindone (**4**) and β-catenin using LIGPLOT software (Figure 4) revealed that the good cytotoxic activity possessed by morindone (**4**) may be attributed to the intermolecular interaction between the compound and the important residues in β-catenin.

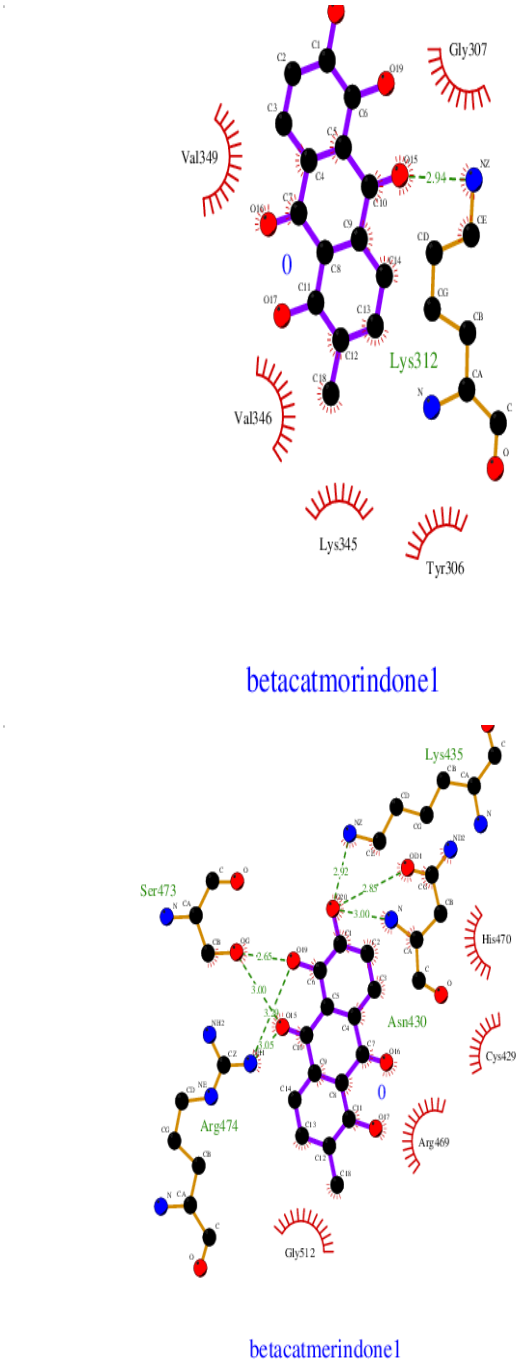

Figure 4: Two- dimensional diagram of binding interaction of the docked structure of morindone **(4)** with β-catenin (PDB ID: 1JDH) protein receptor. A: between morindone (4) and residues at Site A. B: Between analysis of morindone (4) and residues at Site B.

In Site A, the carbonyl oxygen of morindone (**4**) was observed to interact through hydrogen bonding with Lys312 (2.94Å). Hydrophobic interactions also existed between morindone (4) and other residues such as Gly307, Tyr306, Lys345, Val 346 and Val 349 in Site A. Meanwhile, in Site B, the hydroxyl oxygen of compound **4** was hydrogen bonded with Lys435 (2.92Å). Hydrophobic interactions also existed between morindone (**4**) and other residues such as His470, Cys429, Arg469 and Gly512 in Site B. This might lead to a strong interaction inhibition between β-catenin and TCF4. Such interaction was not seen in other docked complex of the anthraquinone derivatives tested in this study with β-catenin. In re-docking experiment on site A of β-catenin the protein-ligand binding interaction analysis showed that isorhamnetin and compound 4 (Figure 5) not only occupied in the same pocket, but also have similar structure orientation.

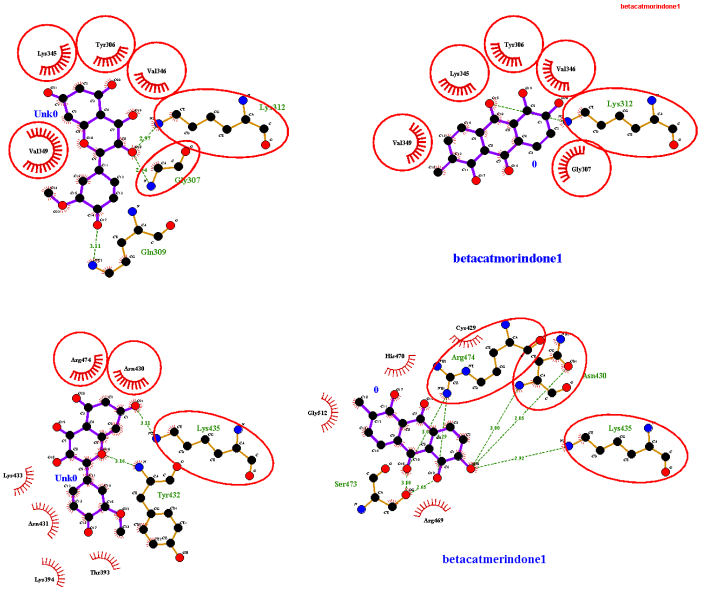

Figure 5: The interaction forces in binding site between isorhamnetin (A) and morindone (**4**) with β-catenin in colon cancer LS174T in active A: site A. B: site B. The common residues are circled.

This is because both compounds were attached to similar residues such as Lys312, Val349, Lys345, Try306, Val346 and Gly307. On the other hand, both compounds were interacting to only 3 similar residues in site B, including Lys435, Arg474 and Asn430. It showed that compound that has almost similar structure orientation with isorhamnetin led to high cytotoxic activity against β-catenin. The formyl moiety in nordamnacanthal (**1**) and damnacanthal (**2**) contributed to the interaction with residues in β-catenin protein. In nordamnacanthal (**1**) two hydrogen bonds were observed between Lys312 and oxygen atom of the chelated hydroxyl group (3.10 Å) and carbonyl group (2.93 Å). Meanwhile, Lys 435 gave a hydrogen bond interaction with the oxygen of the formyl group (2.83Å) in compound 1. Meanwhile, damnacanthal (**2**) only showed hydrogen bond with Lys 312. In compound 67, Lys 312 connected via hydrogen bond with the methoxy oxygen (3.15 Å) and the carbonyl group oxygen (3.05 Å). The anthraquinones can easily substitute in active side B pocket due

to its small molecule characteristics. The LIGPLOT analyses for these compounds are shown in supporting material.

The molecular docking results of nordamnacanthal (**1**) onto Src kinase given by LIGPLOT analysis (Figure 6) showed three intermolecular hydrogen bonds existing between nordamnacanthal (**1**) and the amino acid Mat341 (3.33Å), Thr338 (3.05Å) and Asp404 (2.91Å).

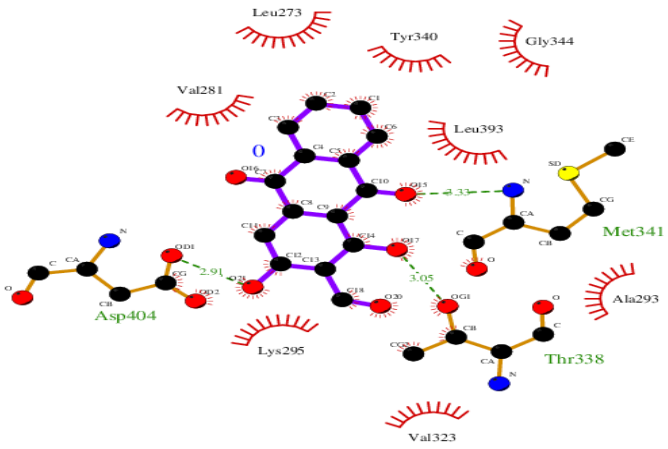

Figure 6: The two-dimensional diagram of binding interaction of the docked structure of nordamnacanthal (**1**) and Src kinase (PDB ID: 2SRC) protein receptor using LIGPLOT [37].

These hydrogen bonds were contributed by oxygen atoms of two hydroxyl groups and one carbonyl group in nordamnacanthal **(1).** Meanwhile the hydrophobic interactions were observed between nordamnacanthal (**1**) with amino acid residues which are Leu273, Try340, Gly344, Val281, Leu393, Lys295, Val323 and Ala293. or hydroxyl and methyl moiety at position C-2 in nordamnacanthal (**1**), damnacanthal (**2**) and damnacanthol (**10**) contributed to hydrogen bonds or hydrophobic interactions with the amino acids in activation loop. Different substituents attached at position C-1 on nordamnacanthal (**1**) and damnacanthal (**2**) resulted in different cytotoxic activities against the K562 cell line. The presence of hydroxyl group in nordamnacanthal (**1**) allows an intermolecular hydrogen bond to be formed, while the methoxyl group in compound 1 contributed to a hydrophobic interaction. The LIGPLOT analysis revealed that there are resemblances in the interacting residues in the Src-kinase-compound **1** complex and Src-kinase-ATP complex (Figure 7).

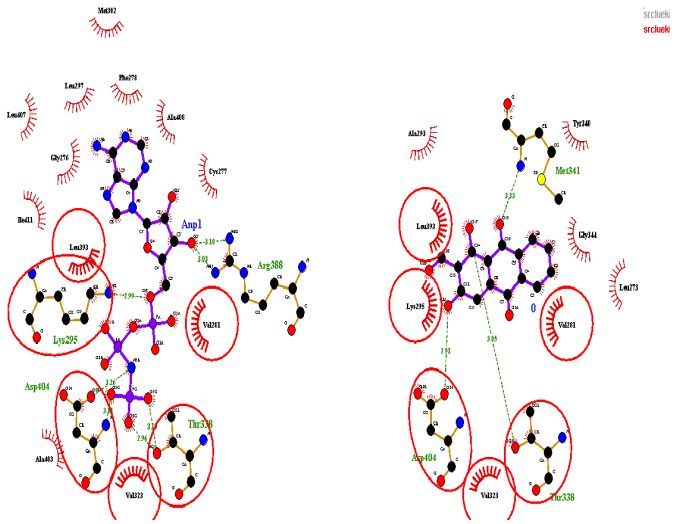

Figure 7: The interaction forces in binding site between Adenosite triphosphate (ATP) and nordamnacanthal (**1**) with with Src protein kinase in leukaemia K562 at active activation loop. The common residues are circled.

There were two hydrogen bonds exist between protein and ligand in both complex; one involving Asp404 and the other one was with Thr338. Meanwhile, the binding of both compounds was also assisted by four hydrophobic interactions with residues such as Leu393, Lys295, Val323 and Val281.

Conclusion

In conclusion, morindone (**4**) showed strong inhibition activities towards SNU-1 and LS-174T cancer cells while nordamnacanthal (**1**) actively inhibit K562 cell line in comparison to the other anthraquinones. This activity was influenced by the types of substituents and their sites of attachment in the anthraquinone skeleton. Molecular docking result showed that all the active compounds can bind well into each targeted protein receptor by binding to important residues in the protein, explaining their inhibitory activities. A detailed work on in-vitro and in-vivo assays towards these two compounds are needed for the development of potential lead compound against SNU-1, LS-174T and K562 cells.

References

1. Samoylenko V, Zhao J, Dunbar DC, Khan IA, Rushing JW, Muhammad I (2006) New constituents from noni (*Morinda citrifolia*) fruit juice. J Agric Food Chem 54: 6398-6402.

2. Wong KM (1984) A synopsis of *Morinda* (Rubiaceae) in the Malay Peninsula, with two new species. Malayan Nat J 38: 89-98.

3. Kamiya K, Tanaka Y, Endang H, Umar M, Satake T (2004) Chemical Constituents of *Morinda citrifolia* Fruits Inhibit Copper-Induced Low-Density Lipoprotein Oxidation. J Agric Food Chem 52: 5843-5848.

4. Kiazolu JB, Intisar A, Zhang L, Wang Y, Zhang R, et al. (2016) Phytochemical screening and chemical variability in volatile oils of aerial parts of *Morinda morindoides*. Nat Prod Res short communication 30: 2249-2252.

5. Olajide OA, Awe SO, Makinde JM, Morebise O (1999) Evaluation of the Anti-diabetic Property of *Morinda lucida* Leaves in Streptozotocin-diabetic Rats. J Pharm Pharmacol 51: 1321-1324.

6. Wang MY, West BJ, Jensen CJ, Nowicki D, Su C, et al. (2002) *Morinda citrifolia* (Noni): A literature review and recent advances in Noni research. Acta Pharmacol Sin 12: 1127-1141.

7. Kim H-K, Kwon M-K, Kim J-N, Kim C-K, Lee Y-J, et al. (2010) Identification of novel fatty acid glucosides from the tropical fruit *Morinda citrifolia* L. Phytochem Lett 3: 238-241.

8. WHO 2017, World Health Organization, Cancer, Fact sheet, (Accessed February 20, **2017**).

9. Brand K, Baker AH, Perez-canto A, Porsling A, Sacharjat M, et al. (2000) Treatment of colorectal liver metastases by Adenoviral transfer tissue inhibitor of metalloproteinases-2 into the liver tissue. Cancer Res 60: 5723-5730.

10. Teng L, and Lu J (2013) cMet as a potential therapeutic target in gastric cancer (Review). Int J Mol Med 32: 1247-1254.

11. Mark AH, Tharun L, Muth J, Dancau AM, Simon R, et al. (2009) HER-2 amplication is highly homogeneous in gastric cancer. Hum Pathol 40: 769-777.

12. Fatima S, Lee NP, Luk JM (2011) Dickkopfs and Wnt/β-catenin signalling in liver cancer. World J Clin Oncol 2: 311-325.

13. Anantharaman A, Subramanian B, Chandrasekaran R, Seenivasan R, Siva R (2014) Colorants and cancer: A review Ind Crops Prod 53: 167-186.

14. Wang MY, West BJ, Jensen CJ, Nowicki D, Su C, et al. (2002) *Morinda citrifolia* (Noni): A literature review and recent advances in Noni research. Acta Pharmacol Sin 12: 1127-1141.

15. Belkis A-A, Kaan Y, Zeynep K, Ahmet CT, Hazal G, et al. (2016) Screening of new antileukemic agents from essential oils of algae extracts and computational modeling of their interactions with intracellular signaling nodes. Eur J Pharm Sci 83: 120-131.

16. Schulz WA (2015) Molecular biology of human cancer: An advanced student's textbook, Springer science + Business media Inc USA.

17. Li H, Chen JD (1998**)** The receptor-associated coactivator 3 activates transcription through CREB-binding protein recruitment and autoregulation. J Biol Chem 273: 5948-5954.

18. Colo GP, Rosato RR, Grant S, Costas MA (2007) RAC3 down-regulated sentizes human chronic myloid leukimia cell to TRAIL-induced apoptosis. FEBS lett 581: 5075-5081.

19. Prista LN, Roque AS, Ferreira MA, Alves AC (1965) Chemical study of *Morinda geminates*. I. Isolation of morindone, damnacanthal, nordamnacanthal and rubiadin-1-methyl ether. Garcia de Orta 13: 19-38.

20. Kamiya K, Tanaka Y, Endang H, Umar M, Satake T (2004) Chemical Constituents of Morinda citrifolia Fruits Inhibit Copper-Induced Low-Density Lipoprotein Oxidation. J Agric Food Chem 52: 5843-5848.

21. Horie Y (1956) Synthesis of damnacanthol and damnacanthal. Yakugaku Zasshi 76: 1448-1449.

22. Simonsen JL, LXVI- Morindone (1918) J. Chem. Soc trans *113*, 766-774.

23. Wijnsma R, Verpoorte R, Mulder-Kriegerand T, Baerheimsvendse A (1984) Anthraquinones in callus cultures of Cinchona ledgerlana. Phytochemistry 23: 2307-2311.

24. Briggs LH, Nicholls GA, Peterson RML (1952) Chemistry of the Coprosma genus. VI Minor anthraquinone colouring matters from Cosprosma australlis. J. Chem Soc 1718-1722.

25. Chari VM, Neelakantan S, Seshadri TR, Rubidin (1966) India J Chem 4: 330-331.

26. Algra RE, Graswinckel WS, Van Enckevort WJP, Vlieg E (2005) Alizarin crystals: An extreme case of solvent induced morphology change J Cryst Growth 285: 168-177.

27. Badr JM (2008) Antioxidant and antimicrobial constituents of Crucianella maritima L Nat Pro Sci 14: 227-232.

28. Roberge G, Brassard P (1981**)** Reactions of ketene acetals13. Synthesis of contiguously Trihydroxylated naphtha and Antraquinones J org Chem 46: 4161-4166.

29. Chang P, Lee KH (1984) Cytotoxic antileukimic antraquinones from *Morinda parvifolia*. Phytochemistry 23: 1733-1736.

30. Halgren TA (1999) MMFF VI. MMFF94s Option for Energy Minimization Studies. J Comput Chem 20: 720-729.

31. Hanwell MD, Curtis DE, Lonie DC, Vandermeersch T, Zurek E, et al. (2012) Avogadro: an advanced semantic chemical editor, visualization, and analysis platform. J Cheminf 4: 17.

32. Sanner MF (1999) Python: a programming language for software integration and development. J Mol Graphics Modell 17: 57-61.

33. Trott O, Olson AJ (2010) AutoDock Vina: improving the speed and accuracy of docking with a new scoring function: efficient optimization and multithreading. J Comput Chem 31: 455-461.

34. Liu J, Wang H, Zuo Y, Farmer SR (2006) Functional Interaction between peroxisome proliferation-activated receptor γ and β-catenin. Mol Cell Biol 26: 5827-5837.

35. Iftikhar H, Rashid S (2004) Molecular docking studies of flavonoids for their inhibition pattern against β-catenin and pharmacophore model generation from experimentally know flavonoids to fabricate more potent inhibitors for Wnt Singnaling pathway. Pharmacognosy magazine 10: 264-271.

36. Park S, Choi J (2010) Inhibition of β-Catenin/Tcf signalling by flavonoids. J Cell Biochem 110: 1376-1385.

37. Laskowski RA, Swindells MB (2011) LigPlot+ : Multiple Ligand-Protein Interaction Digram for Drug Discovery. J Chem Inf Model 51: 2778-2786.

38. Teh SS, Ee GCL, Mah SH, Ahmad Z (2016) Structure-activity relationship study of secondary metabolites from *Mesua beccariana, Mesua ferrea* and *Mesua congestiflora* for anti-cholinesterase activity. Med Chem Res 25: 819-823.

39. Gately DP, Howell SB (1993) Cellular accumulation of the anticancer agent cisplatin: A review. Br J Cancer 67: 1171-1176.

40. Yoo BC, Ku JL, Hong SH, Shinj YK, Park SY, et al. (2003) Decreased pyruvate kinase M2 activity linked to CISPLATIN resistance in human gastric carcinoma cell lines. Int J Cancer 108: 532-539.

41. Otto AM, Brischwein M, Motrescu E, Wolf B (2004) Analysis of drug action on tumor cell metabolism using electronic sensor chips. Arch Pharm Pharm Med Chem 337: 682-686.

42. Chang P, Lee KH (1984**)** Cytotoxic antileukimic antraquinones from *Morinda parvifolia*. *Phytochemistry* 23: 1733-1736.

43. Ali AM, Ismail NH, Mackeen MM, Yazan LS, Mohamed, et al. (2000) Antiviral, Cyototoxic And Antimicrobial Activities Of Anthraquinones Isolated From The Roots Of *Morinda Elliptica*. Pharm Biol 38: 298-301.

44. Tian FF, Jiang FL, Han XL, Xiang C, Ge YS, et al. (2010) Synthesis of a Novel Hydrazone Derivative and Biophysical Studies of Its Interactions with Bovine Serum Albumin by Spectroscopic, Electrochemical, and Molecular Docking Methods. J Phys Chem B 114: 14842-14853.

45. Yuan Q, He L, Ke H (2012) A potential substrate binding conformation of β-Lactams and insight into the broad spectrum of NDM-1 Activity. Antimicrob Agents Chemother 56: 5157-5163.

46. Larsen CA, Bisson WH, Dashwood RH (2009) Tea catechins inhibit hepatocyte growth factor receptor (MET kinase) activity in Human colon cancer cells: kinetics and molecular docking studies. J Med Chem 52: 6543-6545.

47. Graham TA, Ferkey DM, Mao F, Kimelman D, Xu W (2001) Tcf4 can specifically recognize beta-catenin using alternative conformations. Nat Struct Biol 8: 1048-1052.